Distribution of electromagnetic field and group velocities in two-dimensional periodic systems with dissipative metallic components

Vladimir Kuzmiak*
Research Institute For Electronic Science, Hokkaido University, Kita-ku, Sapporo 060, Japan

Alexei A. Maradudin
Department of Physics and Astronomy, University of California, Irvine, California 92697
(Received 8 December 1997)

We study the distribution of the electromagnetic field of the eigenmodes and corresponding group velocities associated with the photonic band structures of two-dimensional periodic systems consisting of an array of infinitely long parallel metallic rods whose intersections with a perpendicular plane form a simple square lattice. We consider both nondissipative and lossy metallic components characterized by a complex frequency-dependent dielectric function. Our analysis is based on the calculation of the complex photonic band structure obtained by using a modified plane-wave method that transforms the problem of solving Maxwell's equations into the problem of diagonalizing an equivalent non-Hermitian matrix. In order to investigate the nature and the symmetry properties of the eigenvectors, which significantly affect the optical properties of the photonic lattices, we evaluate the associated field distribution at the high symmetry points and along high symmetry directions in the two-dimensional first Brillouin zone of the periodic system. By considering both lossless and lossy metallic rods we study the effect of damping on the spatial distribution of the eigenvectors. Then we use the Hellmann-Feynman theorem and the eigenvectors and eigenfrequencies obtained from a photonic band-structure calculation based on a standard plane-wave approach applied to the nondissipative system to calculate the components of the group velocities associated with individual bands as functions of the wave vector in the first Brillouin zone. From the group velocity of each eigenmode the flow of energy is examined. The results obtained indicate a strong directional dependence of the group velocity, and confirm the experimental observation that a photonic crystal is a potentially efficient tool in controlling photon propagation. [S0163-1829(98)02835-5]

I. INTRODUCTION

Recently, it has been demonstrated both theoretically and experimentally that the nature of the wave function associated with the eigenmodes propagating in a photonic crystal significantly affects the optical properties of the photonic crystal. For example, the presence of uncoupled modes in a photonic crystal, whose field patterns display a mismatch with the field pattern of an incoming wave, has been studied by several authors.[1–3] A group theoretical analysis based on the symmetry of two-dimensional lattices shows that some of the observed opaque regions in transmission experiments are artifacts of the measurement in contrast to those that exist due to the band gaps.[1,2] The optical response that occurs in a photonic crystal provides another example of the importance of complete knowledge about the eigenfunctions. Specifically, the intensity of radiation from an oscillating dipole embedded in a photonic crystal depends on position because both the amplitude of the electromagnetic field and the coupling strength between the dipole and the radiation field are position-dependent functions.[4] These two examples clearly demonstrate that the nature of the wave function significantly affects the optical properties of photonic crystals, and that a detailed knowledge of the eigenfunctions is necessary to understand the transport properties of the electromagnetic radiation in these structures.

We recently studied the propagation of electromagnetic waves in both one- and two-dimensional periodic systems with lossy metallic components, and predicted remarkable features occurring in these structures.[5] Namely, we showed that both the lifetime and the absorption coefficient associated with the modes propagating through a one-dimensional system display singular behavior near the band edges. The origin of the former effect was identified as the redistribution of the electromagnetic field in the modes at the bottom and the top of the gap. Another interesting property of a complex photonic band structure is the existence of branches of the lifetimes associated with modes of different symmetry separated by a gap that vanishes as the filling fraction of the rods is increased.

In this paper, we deal with phenomena related to the propagation of electromagnetic waves and the transport of energy through two-dimensional photonic crystals consisting of an array of infinitely long parallel metallic cylinders. In order to obtain deeper physical insight into the nature of phenomena associated with the presence of dissipation, we study the distribution of the electromagnetic fields in terms of the eigenmodes that correspond to the individual bands. We inspect the symmetry of the bands at the points of high symmetry and along the high symmetry directions in the two-dimensional first Brillouin zone of the photonic crystal. By evaluating the eigenfunctions, we identify uncoupled modes, and we also determine the symmetry of modes in the cases in which a definite symmetry cannot be assigned by the use of group theory itself. Furthermore, we evaluate the group velocity associated with the individual eigenmodes al-

lowed within the photonic crystal, in particular at the band edges, since in these regions the Ioffe-Regel criterion is satisfied, which consequently may give rise to the existence of phenomena related to the localization of light.[6]

The present paper is organized as follows. In Sec. II we briefly describe the linearization technique used to calculate the complex photonic band structure, and we apply the Hellmann-Feynman theorem to obtain an expression for the group velocity of the individual bands. In Sec. III, we present the results obtained by applying these methods to the system that consists of infinitely long lossy metallic rods, whose intersections with a perpendicular plane form a square lattice. In particular, we focus on the effect of the presence of dissipation on the nature of the spatial distribution of the electric field associated with the individual bands at the points of high symmetry in the first Brillouin zone, and on the dependence of the group velocities associated with the individual bands of the photonic band structure of the system with lossless metallic rods, on their filling fraction. The interpretation of the interesting features associated with the complex valued dispersion law and possible directions for future research are presented in Sec. IV.

II. COMPUTATIONAL METHOD

A. Evaluation of the complex photonic band structure

The physical system that we consider in this paper consists of infinitely long, identical, metallic rods, whose intersections with a plane perpendicular to the rods form a two-dimensional lattice. We first consider lossless metallic cylinders characterized by a simple free-electron dielectric function of the form

$$\epsilon(\omega)=1-\frac{\omega_p^2}{\omega^2}, \tag{2.1}$$

where the plasma frequency ω_p is typically in the ultraviolet frequency region.

To calculate the photonic band structure for the modes propagating through the system consisting of metallic rods without dissipation we employ the modified plane-wave method developed by the present authors.[7] We simultaneously study the system with lossy components when dissipation is introduced through the use of a dielectric function of the form

$$\epsilon(\omega)=1-\frac{\omega_p^2}{\omega(\omega+i\gamma)}, \tag{2.2}$$

where the parameter γ is an inverse electronic relaxation time.

The vector electromagnetic field in a two-dimensional (2D) photonic crystal can be decoupled into two independent polarization components,[8] viz., *E* polarization, in which the electric field is parallel to the axes of the rods, and *H* polarization, in which the magnetic field is parallel to the axes of the rods. In this paper, we will deal with the *E*-polarized electromagnetic waves propagating through a two-dimensional photonic crystal formed by an array of infinitely long metallic cylinders of circular cross section surrounded by vacuum, whose intersections with a perpendicular plane form a simple square lattice of lattice parameter *a*. We assume that the axes of the cylinders are parallel to the x_3 axis and the positions of the sites of this lattice are given by the vectors

$$\mathbf{x}_\parallel(l)=l_1\mathbf{a}_1+l_2\mathbf{a}_2, \tag{2.3}$$

where $\mathbf{a}_1=a(1,0,0)$ and $\mathbf{a}_2=a(0,1,0)$ are the two, noncolinear, primitive translation vectors of the lattice, while l_1 and l_2 are arbitrary integers that we denote collectively by *l*. The area a_c of a primitive unit cell of this lattice is given by $a_c=|\mathbf{a}_1\times\mathbf{a}_2|=a^2$.

The lattice reciprocal to the direct lattice whose points are defined by Eq. (2.3) is defined by the translation vectors

$$\mathbf{G}_\parallel(h)=h_1\mathbf{b}_1+h_2\mathbf{b}_2, \tag{2.4}$$

where $\mathbf{b}_1=(2\pi/a)(1,0,0)$ and $\mathbf{b}_2=(2\pi/a)(0,1,0)$ are the primitive translation vectors of the reciprocal lattice, and h_1 and h_2 are arbitrary integers that we denote collectively by *h*.

The system we study is characterized by a position-dependent dielectric function of the form

$$\epsilon[\mathbf{x}_\parallel+\mathbf{x}_\parallel(l)|\omega]=\epsilon(\mathbf{x}_\parallel|\omega), \tag{2.5}$$

where $\mathbf{x}_\parallel=(x_1,x_2,0)$ is two-dimensional vector in the x_1x_2 plane and $\epsilon(\mathbf{x}_\parallel|\omega)$ is a position-dependent, periodic function of $\mathbf{x}_\parallel$ with the periodicity of the Bravais lattice defined by Eq. (2.3). It can therefore be expanded in a two-dimensional Fourier series according to

$$\epsilon(\mathbf{x}_\parallel|\omega)=\sum_{\mathbf{G}_\parallel}\hat{\epsilon}(\mathbf{G}_\parallel)e^{i\mathbf{G}_\parallel\cdot\mathbf{x}_\parallel}, \tag{2.6}$$

and in the particular case of cylinders characterized by the dielectric function given by Eq. (2.2), whose cross section is a circle of radius *R* we obtain for the Fourier coefficients $\hat{\epsilon}(\mathbf{G}_\parallel)$,

$$\hat{\epsilon}(\mathbf{G}_\parallel)=\begin{cases}1-f\dfrac{\omega_p^2}{\omega(\omega+i\gamma)}, & \mathbf{G}_\parallel=\mathbf{0} \quad (2.7a)\\[2ex] -f\dfrac{\omega_p^2}{\omega(\omega+i\gamma)}\dfrac{2J_1(G_\parallel R)}{(G_\parallel R)}, & \mathbf{G}_\parallel\neq\mathbf{0}. \quad (2.7b)\end{cases}$$

Here $f=\pi R^2/a^2$ is the filling fraction, i.e., the fraction of the volume occupied by the rods, and $J_1(x)$ is a Bessel function.

In the case of *E* polarization, we seek solutions of the Maxwell equations that have the forms

$$\mathbf{E}(\mathbf{x};t)=(0,0,\mathbf{E}_3(\mathbf{x}_\parallel|\omega))\exp(-i\omega t) \tag{2.8a}$$

$$\mathbf{H}(\mathbf{x};t)=(H_1(\mathbf{x}_\parallel|\omega),H_2(\mathbf{x}_\parallel|\omega),0)\exp(-i\omega t). \tag{2.8b}$$

The Maxwell curl equations for the three nonzero field components are

$$\frac{\partial H_2}{\partial x_1}-\frac{\partial H_1}{\partial x_2}=-i\frac{\omega}{c}D_3=-i\frac{\omega}{c}\epsilon(\mathbf{x}_\parallel|\omega)E_3, \tag{2.9a}$$

$$\frac{\partial E_3}{\partial x_1}=-i\frac{\omega}{c}H_2, \tag{2.9b}$$

$$\frac{\partial E_3}{\partial x_2}=i\frac{\omega}{c}H_1. \tag{2.9c}$$

The equation for E_3 obtained by eliminating H_1 and H_2 from these equations can be written in the form

$$\left(\frac{\partial^2}{\partial x_1^2}+\frac{\partial^2}{\partial x_2^2}\right)E_3+\epsilon(\mathbf{x}_\parallel|\omega)\,\frac{\omega^2}{c^2}\,E_3=0. \tag{2.10}$$

To solve Eq. (2.10) we use the expansion (2.6) and write $E_3(\mathbf{x}_\parallel|\omega)$ in the form

$$E_3(\mathbf{x}_\parallel|\omega)=\sum_{\mathbf{G}_\parallel} B(\mathbf{k}_\parallel|\mathbf{G}_\parallel)e^{i(\mathbf{k}_\parallel+\mathbf{G}_\parallel)\cdot\mathbf{x}_\parallel}, \tag{2.11}$$

where $\mathbf{k}_\parallel=(k_1,k_2,0)$ is the two-dimensional wave vector of the wave. When these expansions and the results for the Fourier coefficients $\hat{\epsilon}(\mathbf{G}_\parallel)$ are substituted into Eq. (2.10), we obtain a polynomial matrix equation satisfied by the coefficients $\{B(\mathbf{k}_\parallel|\mathbf{G}_\parallel)\}$, which takes the form

$$(\mu^3\overleftrightarrow{I}-\mu^2\overleftrightarrow{P}-\mu\overleftrightarrow{Q}-\overleftrightarrow{R})\mathbf{B}=0, \tag{2.12}$$

where the elements of the $NG\times NG$ matrices $\overleftrightarrow{P}$, $\overleftrightarrow{Q}$, and $\overleftrightarrow{R}$ are given by

$$\overleftrightarrow{P}(\mathbf{G}_\parallel|\mathbf{G}_\parallel')=-i\,\frac{\gamma}{c}\,\delta_{\mathbf{G}_\parallel,\mathbf{G}_\parallel'}, \tag{2.13a}$$

$$\overleftrightarrow{Q}(\mathbf{G}_\parallel|\mathbf{G}_\parallel')=(\mathbf{k}_\parallel+\mathbf{G}_\parallel)^2\delta_{\mathbf{G}_\parallel,\mathbf{G}_\parallel'}+f\,\frac{\omega_p^2}{c^2}\,\frac{2J_1(|\mathbf{G}_\parallel-\mathbf{G}_\parallel'|R)}{(|\mathbf{G}_\parallel-\mathbf{G}_\parallel'|R)}, \tag{2.13b}$$

$$\overleftrightarrow{R}(\mathbf{G}_\parallel|\mathbf{G}_\parallel')=i\,\frac{\gamma}{c}\,\delta_{\mathbf{G}_\parallel,\mathbf{G}_\parallel'}(\mathbf{k}_\parallel+\mathbf{G}_\parallel)^2. \tag{2.13c}$$

Here $J_1(x)$ is a Bessel function, and NG is the number of plane waves used in the expansions of $\epsilon(\mathbf{x}_\parallel|\omega)$ and $E_3(\mathbf{x}_\parallel|\omega)$ given by Eqs. (2.6) and (2.11), respectively.

The nonlinear eigenvalue problem given by Eq. (2.12) can be transformed into a linear problem in $3NG$ dimensions by using a standard linearization technique based on the construction of an equivalent matrix $\overleftrightarrow{W}(\mathbf{G}_\parallel|\mathbf{G}_\parallel')$ given by[9]

$$\overleftrightarrow{W}(\mathbf{G}_\parallel|\mathbf{G}_\parallel')=\begin{bmatrix}\overleftrightarrow{0} & \overleftrightarrow{I} & \overleftrightarrow{0}\\ \overleftrightarrow{0} & \overleftrightarrow{0} & \overleftrightarrow{I}\\ \overleftrightarrow{R} & \overleftrightarrow{Q} & \overleftrightarrow{P}\end{bmatrix}. \tag{2.14}$$

Thus, the solution of Eq. (2.12) is reduced to the diagonalization of the complex, non-Hermitian matrix $\overleftrightarrow{W}$, which yields complex eigenvalues that can be expressed in the form

$$\mu=\frac{\omega_R}{c}+i\,\frac{\omega_I}{c}, \tag{2.15}$$

where ω_R represents the real part of the complex frequency, and ω_I determines the lifetime of the mode τ according to the definition

$$\frac{1}{\tau}=-2\,\omega_I. \tag{2.16}$$

It is well known from matrix theory that the non-Hermiticity of the matrix $\overleftrightarrow{W}(\mathbf{G}_\parallel|\mathbf{G}_\parallel')$ implies the existence of nonidentical right and left eigenvectors $\mathbf{B}^{(R)}$, $\mathbf{B}^{(L)}$, which satisfy the equations

$$\sum_{\mathbf{G}_\parallel'}\overleftrightarrow{W}(\mathbf{G}_\parallel|\mathbf{G}_\parallel')\mathbf{B}^{(R)}(\mathbf{G}_\parallel')=\mu B^{(R)}(\mathbf{G}_\parallel), \tag{2.17a}$$

$$\sum_{\mathbf{G}_\parallel} B^{(L)}(\mathbf{G}_\parallel)^T\overleftrightarrow{W}(\mathbf{G}_\parallel|\mathbf{G}_\parallel')=\mu B^{(L)}(\mathbf{G}_\parallel')^T. \tag{2.17b}$$

Both the right and left eigenvectors that satisfy Eqs. (2.17a) and (2.17b) can be expressed in terms of three vectors each of which has NG components. Therefore, we can rewrite the latter equations in the forms

$$\begin{pmatrix}\overleftrightarrow{0} & \overleftrightarrow{I} & \overleftrightarrow{0}\\ \overleftrightarrow{0} & \overleftrightarrow{0} & \overleftrightarrow{I}\\ \overleftrightarrow{R} & \overleftrightarrow{Q} & \overleftrightarrow{P}\end{pmatrix}\begin{pmatrix}\mathbf{B}_\alpha^{(R)}\\ \mathbf{B}_\beta^{(R)}\\ \mathbf{B}_\gamma^{(R)}\end{pmatrix}=\mu\begin{pmatrix}\mathbf{B}_\alpha^{(R)}\\ \mathbf{B}_\beta^{(R)}\\ \mathbf{B}_\gamma^{(R)}\end{pmatrix} \tag{2.18a}$$

and

$$(\mathbf{B}_\alpha^{(L)T},\mathbf{B}_\beta^{(L)T},\mathbf{B}_\gamma^{(L)T})\begin{pmatrix}\overleftrightarrow{0} & \overleftrightarrow{I} & \overleftrightarrow{0}\\ \overleftrightarrow{0} & \overleftrightarrow{0} & \overleftrightarrow{I}\\ \overleftrightarrow{R} & \overleftrightarrow{Q} & \overleftrightarrow{P}\end{pmatrix}=\mu(\mathbf{B}_\alpha^{(L)T},\mathbf{B}_\beta^{(L)T},\mathbf{B}_\gamma^{(L)T}), \tag{2.18b}$$

respectively. Now we use the partitioned form of the matrix $\overleftrightarrow{W}$ in Eq. (2.18a) to obtain the eigenvalue equations satisfied by the vectors $\mathbf{B}_\alpha^{(R)}$, $\mathbf{B}_\beta^{(R)}$, $\mathbf{B}_\gamma^{(R)}$ in the form

$$\mathbf{B}_\beta^{(R)}=\mu\mathbf{B}_\alpha^{(R)}, \tag{2.19a}$$

$$\mathbf{B}_\gamma^{(R)}=\mu\mathbf{B}_\beta^{(R)}, \tag{2.19b}$$

$$\overleftrightarrow{R}\mathbf{B}_\alpha^{(R)}+\overleftrightarrow{Q}\mathbf{B}_\beta^{(R)}+\overleftrightarrow{P}\mathbf{B}_\gamma^{(R)}=\mu\mathbf{B}_\gamma^{(R)}. \tag{2.19c}$$

By eliminating the vectors $\mathbf{B}_\alpha^{(R)}$ and $\mathbf{B}_\gamma^{(R)}$ from the latter equations we obtain the polynomial matrix equation satisfied by vector $\mathbf{B}_\beta^{(R)}$,

$$(\mu^3\overleftrightarrow{I}-\mu^2\overleftrightarrow{P}-\mu\overleftrightarrow{Q}-\overleftrightarrow{R})B_\beta^{(R)}=0, \tag{2.20}$$

which corresponds to the original polynomial matrix equation given by Eq. (2.12). The eigenvectors $\mathbf{B}_\beta^{(R)}$ yield eigenvalues, which possess a positive real component and a negative imaginary component and, therefore, correspond to physical modes.

In the following we show that both right and left eigenvectors yield equivalent solutions, so that in inspecting the spatial distribution of the modes we can restrict ourselves to either of the two eigenvectors $\mathbf{B}_\beta^{(R)}$ or $\mathbf{B}_\gamma^{(L)T}$.

In order to prove the latter statement we again use the partitioned form of the matrix $\overleftrightarrow{W}$ in Eq. (2.18b) to obtain the eigenvalue equations satisfied by the vectors $\mathbf{B}_\alpha^{(L)T}$, $\mathbf{B}_\beta^{(L)T}$, $\mathbf{B}_\gamma^{(L)T}$:

$$\mathbf{B}_\gamma^{(L)T}\overleftrightarrow{R}=\mu\mathbf{B}_\alpha^{(L)T}, \tag{2.21a}$$

$$\mathbf{B}_\alpha^{(L)T}+\mathbf{B}_\gamma^{(L)T}\overleftrightarrow{Q}=\mu\mathbf{B}_\beta^{(L)T}, \tag{2.21b}$$

$$\mathbf{B}_{\beta}^{(L)T}+\mathbf{B}_{\gamma}^{(L)T}\vec{\vec{P}}=\mu\mathbf{B}_{\gamma}^{(L)T}. \tag{2.21c}$$

By eliminating the vectors $\mathbf{B}_{\alpha}^{(L)T}$ and $\mathbf{B}_{\beta}^{(L)T}$ in these equations we obtain the polynomial matrix equation satisfied by vector $\mathbf{B}_{\gamma}^{(L)T}$,

$$\mathbf{B}_{\gamma}^{(L)T}(\mu^3\vec{\vec{I}}-\mu^2\vec{\vec{P}}-\mu\vec{\vec{Q}}-\vec{\vec{R}})=0. \tag{2.22}$$

By taking the transpose of this equation and keeping in mind that the matrices $\vec{\vec{P}},\vec{\vec{Q}},\vec{\vec{R}}$ defined by Eqs. (2.13a), (2.13b), and (2.13c) are symmetric, we obtain an equation that corresponds to the polynomial equation (2.20) that is satisfied by the eigenvector $\mathbf{B}_{\beta}^{(R)}$. Hence, we have proved the equivalence of the solutions associated with the eigenvectors $\mathbf{B}_{\beta}^{(R)}$ and $\mathbf{B}_{\gamma}^{(L)T}$.

Using the solutions given by the eigenvalues with a positive real component and a negative imaginary component associated with right eigenvectors we inspect the spatial distributions of the electromagnetic fields that correspond to the physical modes. We focus on the evaluation of the spatial distribution associated with the high symmetry points of the first Brillouin zone, in particular with respect to the interesting features, which we have found for the lifetimes of the modes determined from the imaginary part of the complex photonic band structure.[5]

B. Group velocity calculation

To study the energy transfer associated with the individual eigenmodes allowed in our two-dimensional model system we evaluate the group velocities of the individual bands. In general, the direction of wave propagation can be determined by inspecting the propagation of a wave packet in space and time. When the wave packet propagates through a medium characterized by a real-valued dispersion law $\omega(\mathbf{k})$, it can be shown that the velocity of the energy flow, including its direction, is given by the group velocity $\mathbf{v}_g=\nabla_{\mathbf{k}}\omega(\mathbf{k})$.[10–12] In this paper, we examine the group velocity $\mathbf{v}_g^{\mu}(\mathbf{k}_{\|})=\nabla\omega_{\mu}(\mathbf{k}_{\|})$ associated with the μth band of the photonic band structure for waves propagating through a two-dimensional photonic crystal with lossless metallic components. In the case of *E*-polarized waves we can calculate the group velocity by using the Hellmann-Feynman theorem and the corresponding dispersion relation, which can be written in the form a of standard eigenvalue problem[7]

$$\sum_{\mathbf{G}_{\|}'} M_E(\mathbf{k}_{\|}+\mathbf{G}_{\|}|\mathbf{k}_{\|}+\mathbf{G}_{\|}')A(\mathbf{k}_{\|}|\mathbf{G}_{\|}')=\frac{\omega^2}{c^2}A(\mathbf{k}_{\|}|\mathbf{G}_{\|}), \tag{2.23}$$

where the matrix element $M_E(\mathbf{k}_{\|}+\mathbf{G}_{\|}|\mathbf{k}_{\|}+\mathbf{G}_{\|}')$ is given by

$$M_E(\mathbf{k}_{\|}+\mathbf{G}_{\|}|\mathbf{k}_{\|}+\mathbf{G}_{\|}')=(\mathbf{k}_{\|}+\mathbf{G}_{\|})^2\delta_{\mathbf{G}_{\|},\mathbf{G}_{\|}'}+f\frac{\omega_p^2}{c^2}\frac{2J_1(|\mathbf{G}_{\|}-\mathbf{G}_{\|}'|R)}{(|\mathbf{G}_{\|}-\mathbf{G}_{\|}'|R)}, \tag{2.24}$$

$J_1(x)$ is a Bessel function, and $f=\pi R^2/a^2$ is the filling fraction, i.e., the fraction of the total volume occupied by the metallic rods, which are assumed to have a circular cross section of radius *R*.

When the Hellmann-Feynman theorem is applied to the eigenvalue problem we obtain the jth component of the group velocity $v_g(\mathbf{k}_{\|})$ associated with the μth band in the form

$$v_{gj}^{\mu}(\mathbf{k}_{\|})=\frac{\partial}{\partial k_j}\omega_{\mu}(\mathbf{k}_{\|})=\frac{c^2}{2\omega_{\mu}(\mathbf{k}_{\|})}\sum_{\mathbf{G}_{\|},\mathbf{G}_{\|}'}A^{\mu}(\mathbf{k}_{\|}|\mathbf{G}_{\|})\frac{\partial M_E(\mathbf{k}_{\|}+\mathbf{G}_{\|}|\mathbf{k}_{\|}+\mathbf{G}_{\|}')}{\partial k_j}\times A^{\mu}(\mathbf{k}_{\|}|\mathbf{G}_{\|}'),\quad j=1,2, \tag{2.25}$$

where $\omega_{\mu}(\mathbf{k}_{\|})$ are the eigenvalues associated with the μth band.

III. RESULTS

A. The distribution of the EM field at high symmetry points in the first Brillouin zone in a system of metallic rods without damping

Let us first consider the symmetry of the bands in the photonic band structure for *E*-polarized electromagnetic waves propagating through a system of lossless metallic rods characterized by the dielectric function Eq. (2.1), arrayed in a simple square lattice, when the filling fraction of the rods is $f=0.1$. In Fig. 1 we present the photonic band structure for the electromagnetic waves propagating through this system. The dispersion curves shown in Fig. 1 demonstrate a characteristic feature of the dispersion law for photonic crystals with metallic components, namely, the existence of an acoustic gap from zero frequency up to a cutoff frequency ω_c. To analyze the nature of the individual modes of the photonic band structure shown in Fig. 1 we tabulate the spatial distribution of the electric field associated with the eigenfunctions and eigenvalues evaluated at the high symmetry points and along the symmetry directions in the first Brillouin zone. The spatial distribution shown in Fig. 1 is determined from the real component of the electric fields given by Eq. (2.11). In Fig. 1 we indicate systematically the symmetry of the four lowest bands at the high symmetry points and along the M-Γ-X-M directions. The symmetries of some of these bands are explicitly demonstrated by plotting the field patterns shown in Figs. 2–5. The distributions presented in this paper are sampled every $a/20$ in the region of the x_1x_2 plane, which is composed of 2×2 unit cells, each of which has a lattice constant a.

We begin with the field pattern with the symmetry of the irreducible representation B_2 of the point group C_{4v} associated with the lowest state at the M point shown in Fig. 2(a), which is symmetric with respect to the σ_v' reflections and antisymmetric with respect to the σ_v reflections. Here we denote the mirror planes that contain the x_3 axis and intersect the x_1x_2 plane along the x_1, x_2 axes and along the lines $x_1=x_2$, $x_1=-x_2$ by $\sigma_v^{(1)}$, $\sigma_v^{(1)}$ and $\sigma_v'^{(1)}$, $\sigma_v'^{(2)}$, respectively. The second lowest band at the M point, which is doubly

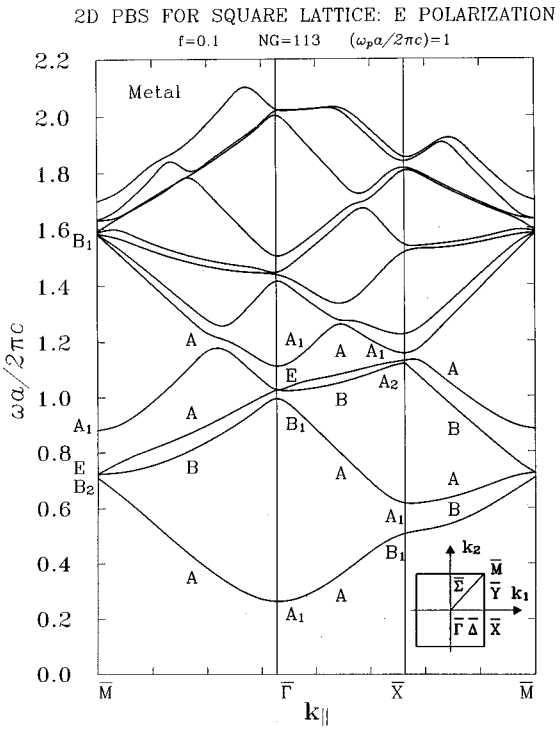

FIG. 1. The photonic band structure of a 2D square lattice consisting of lossless metallic rods in vacuum obtained by the plane-wave method. E polarization, $f=0.1$. The number of plane waves used in these calculations is $NG=113$.

degenerate, reveals rather striking behavior, namely the electric fields associated with this mode, which correspond to the two orthogonal eigenvectors belonging to the E irreducible representation, vanish. This phenomenon is demonstrated in Fig. 2(b) where the vanishing amplitude is indicated by a contour map. In Fig. 2(c), we display a fully symmetric pattern, that corresponds to the distribution of the electric field associated with the third lowest frequency band at the $\bar{M}$ point. In Fig. 3(a), we present the distribution of the electric field associated with the lowest frequency band for the wave vector $\mathbf{k}_{\|}=(0.5,0.5)\pi/a$, which belongs to the irreducible representation A of the point group C_2. In agreement with the compatibility relation the second lowest doubly degenerate mode at the $\bar{M}$ point splits into bands belonging to the irreducible representations B and A of the point group C_2 for the wave vector $\mathbf{k}_{\|}=(0.5,0.5)\pi/a$ along the $\bar{\Gamma}$-$\bar{M}$ direction. The field patterns of these bands shown in Figs. 3(b) and 3(c) demonstrate that the former is antisymmetric with respect to a rotation through π and hence forms an uncoupled mode, while the latter displays fully symmetric behavior.

The eigenfunction associated with the lowest band at the $\bar{\Gamma}$ point shown in Fig. 4(a) displays a field pattern belonging to the irreducible representation A_1 of the point group C_{4v} that possesses a sinelike behavior that peaks between the metallic rods. The second lowest band shown in Fig. 4(b) is a nondegenerate state of B_1 symmetry, which is symmetric with respect to the σ_v mirror reflections along the x_1 and x_2 axes. The third lowest band is a doubly degenerate state of E symmetry. The spatial distribution of the electric field associated with the degenerate modes that correspond to the two orthogonal eigenvectors of the E irreducible representation has a zero amplitude as depicted in Fig. 4(c).

Let us turn now to the X point in the first Brillouin zone. The contour map associated with the lowest band shown in Fig. 5(a) reflects the vanishing amplitude of the wave function, which belongs to the irreducible representation B_1 of the point group C_{2v}. In Fig. 5(b) we present the spatial distribution of the electric field associated with the second lowest band. It is symmetric with respect to a rotation through π and to mirror reflections $\sigma_v^{(2)}$ along the x_1 and x_2 axes, and thus belongs to the irreducible representation A_1 of the point group C_{2v}. Finally, the spatial distribution of the third lowest band shown in Fig. 5(c) is antisymmetric with respect to the σ_v mirror reflections and symmetric with respect to a rotation through π. Hence it is identified as an A_2 state.

The photonic bands of a square lattice composed of circular rods have been classified according to the group theory based on the symmetry of the photonic crystal.[3] Since the position-dependent dielectric constant given by Eq. (2.5) is invariant under the symmetry operations belonging to the point group C_{4v}, a conventional classification of eigenmodes based on group theory is applicable. In Table I we show the symmetries of the M, Γ, and X points and the irreducible representations for several low eigenfrequencies in the case of a square lattice. Table II shows the compability relations between the high symmetry points M, Γ, and X, and the M-Γ and Γ-X directions. The notation such as A_1+B_1+E in Table I means that the mode assignment shown in Table I accomplished by group theory itself does not allow assigning a definite symmetry to each mode. Therefore, it is useful to employ our method based on inspecting the nature of the electric field distributions to determine a definite symmetry of each of the eigenmodes.

B. Effect of dissipation on the distribution of the EM field at high symmetry points in the first Brillouin zone in the system with lossy metallic rods

We now turn to the results for E polarization when dissipation in the metal rods is taken into account by the linearization technique described in Sec. II. We assume the electromagnetic waves propagate through a system of lossy metallic rods arrayed in a simple square lattice with the filling fractions $f=0.01$ and $f=0.1$. In Figs. 6(a)–6(d), we present the photonic band structures and the lifetimes of the modes associated with these band structures. The dispersion curves shown in Fig. 6(c) indicate that the real part of the complex photonic band structure, in comparison with the dispersion curves obtained for the system without dissipation, see Fig. 1, is negligibly affected by the presence of damping when the value of the damping constant γ is small relative to the plasma frequency, e.g., $\gamma=0.01\omega_p$, a typical value for a metal. In Figs. 6(b) and 6(d) we present the lifetimes of the E-polarized modes, which are determined from the imaginary part of the complex eigenvalues obtained by diagonalizing the non-Hermitian matrix $\vec{W}$ $(\mathbf{G}_{\|}|\mathbf{G}_{\|})$ given by Eq. (2.14). The lifetimes depicted in Fig. 6(b) correspond to the 12 lowest eigenmodes and reveal an interesting feature, namely, the existence of branches of lifetimes, which form two regions separated by a gap. The formation of these re-

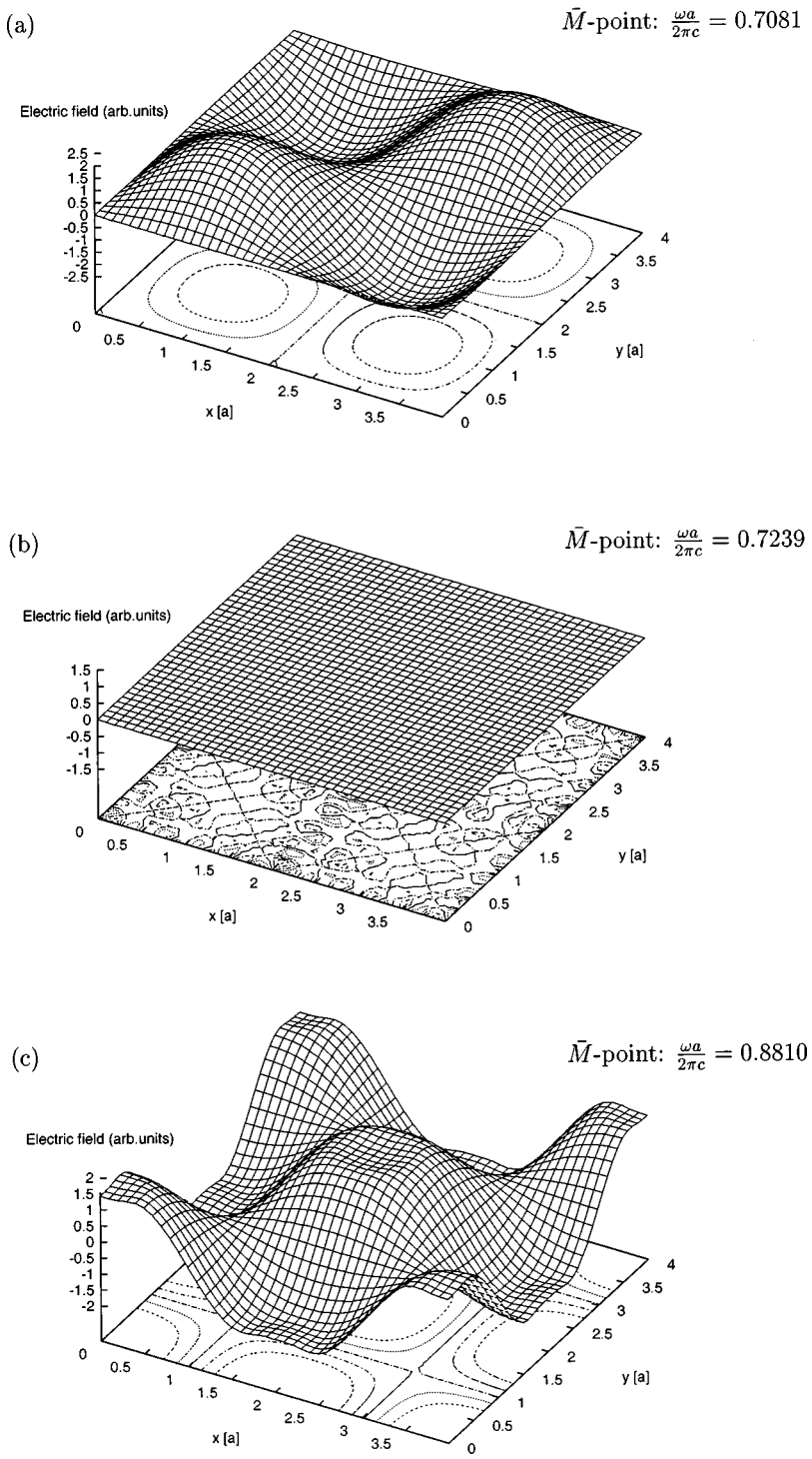

FIG. 2. The electric field distribution associated with the eigenfunctions and eigenvalues that correspond to the photonic band structure shown in Fig. 1, evaluated at the $\bar{M}$ point of the first Brillouin zone, which correspond to the lowest band with the frequency (a) $\omega a/2\pi c = 0.7081$, to the second lowest doubly degenerate state of E symmetry with the frequency (b) $\omega a/2\pi c = 0.7239$, and to the third lowest band with the frequency (c) $\omega a/2\pi c = 0.8810$. The spatial distribution of the electric field associated with the eigenfunctions is tabulated every $a/20$ in the region of the x_1x_2 plane, which is composed of 2×2 square lattice unit cells each of which has a lattice constant a.

gions is illustrated in Fig. 6(e), in which we depict the lifetimes associated with the four lowest bands, where the superscripts correspond to the number of the band. The analysis of the symmetry associated with the bands of the lifetimes reveals that the lifetimes, which form the lower region are associated with the modes that possess A symmetry, while the lifetimes that form the upper region are associated with uncoupled modes of B symmetry, which are antisymmetric with respect to a rotation through π. It is interesting to note that the ordering of the branches of the lifetimes along the high symmetry directions is determined by the symmetries of the modes, which may give rise to the

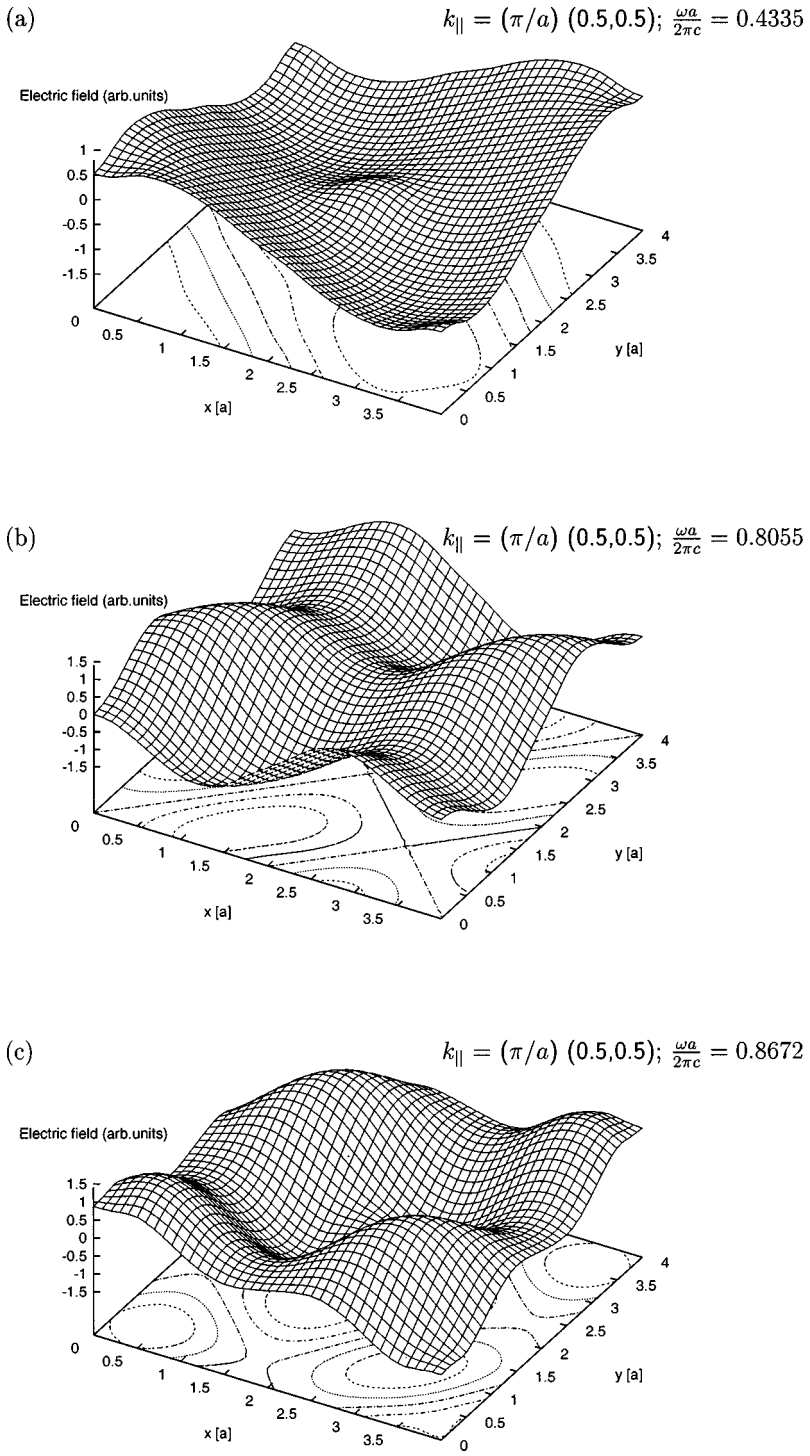

FIG. 3. The electric field distributions associated with the eigenfunctions and eigenvalues that correspond to the photonic band structure shown in Fig. 1, evaluated at the $\mathbf{k}_{\|} = (0.5,0.5)\pi/a$ point along the $\bar{M}$-$\bar{\Gamma}$ direction in the first Brillouin zone, which correspond to the three lowest bands with the frequencies (a) $\omega a/2\pi c = 0.4335$, (b) $\omega a/2\pi c = 0.8055$, and (c) $\omega a/2\pi c = 0.8672$.

discontinuous behavior demonstrated in Fig. 6(e) between the lifetimes segments denoted by $A^{(1)}$ and $B^{(1)}$ associated with the lowest frequency mode along the $\bar{\Gamma}$-$\bar{X}$ and $\bar{X}$-$\bar{M}$ directions, respectively. We found that the forbidden region between the lifetime bands depends strongly on the filling fraction and vanishes as the filling fraction is increased—see Fig. 6(d). To explain the existence of these features we study the eigenfunctions associated with each of the eigenmodes within the context of the variational theorem in electromagnetism, which links the mode frequency with the spatial variation of the electric field.[13]

In order to explore the nature of the eigenmodes we examine the spatial variation of the electromagnetic field associated with eigenvectors that correspond to the physical solutions of the matrix equation (2.12). Since the resulting fields are complex, we plot the intensity of the electric field to display the spatial distributions of the modes propagating in the system in the presence of dissipation. The field pattern

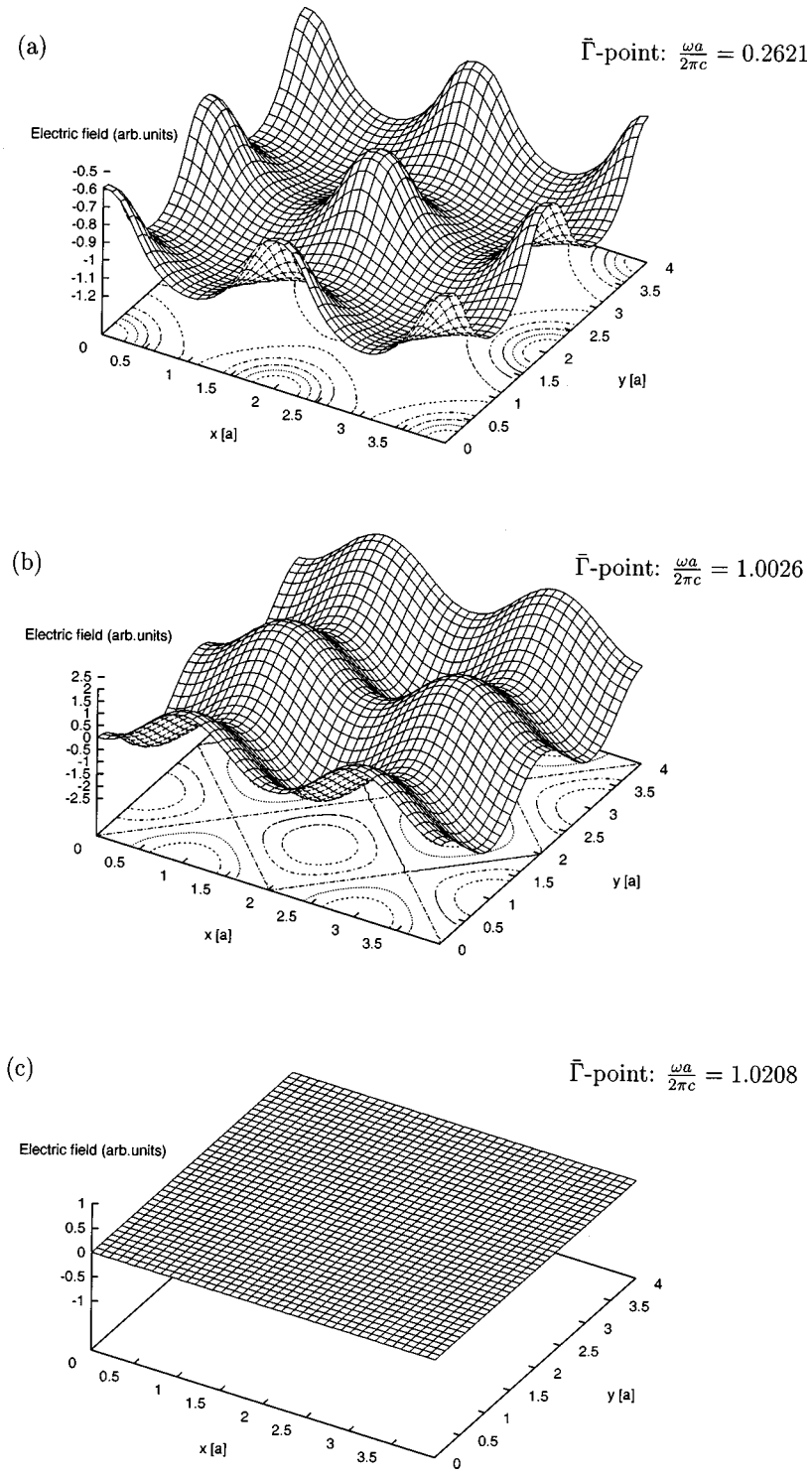

FIG. 4. The electric field distributions associated with the eigenfunctions and eigenvalues that correspond to the photonic band structure shown in Fig. 1, evaluated at the $\bar{\Gamma}$ point in the first Brillouin zone that correspond to the lowest band with the frequency (a) $\omega a/2\pi c = 0.2621$, to the second lowest band with the frequency (b) $\omega a/2\pi c = 1.0026$, and to the third lowest doubly degenerate mode with the frequency (c) $\omega a/2\pi c = 1.0208$.

associated with the intensity of the electric field determined from the eigenvector which correspond to the lowest frequency band at the M point resembles the distribution shown in Fig. 2(a), which displays the dominant variation between the rods. However, the field patterns associated with the intensity of the fields associated with the second lowest doubly degenerate mode at the $\bar{M}$ point shown in Figs. 7(b) and 7(c), exhibit markedly different behavior. While in the system with lossless rods the electric field associated with the second lowest band vanishes for the two orthogonal eigenvectors, the spatial distributions of intensity of the electric fields which correspond to the second lowest, doubly degenerate, band of E symmetry display patterns that are symmetric with respect to the mirror planes $\sigma_v'^{(1)}$ and $\sigma_v'^{(2)}$.

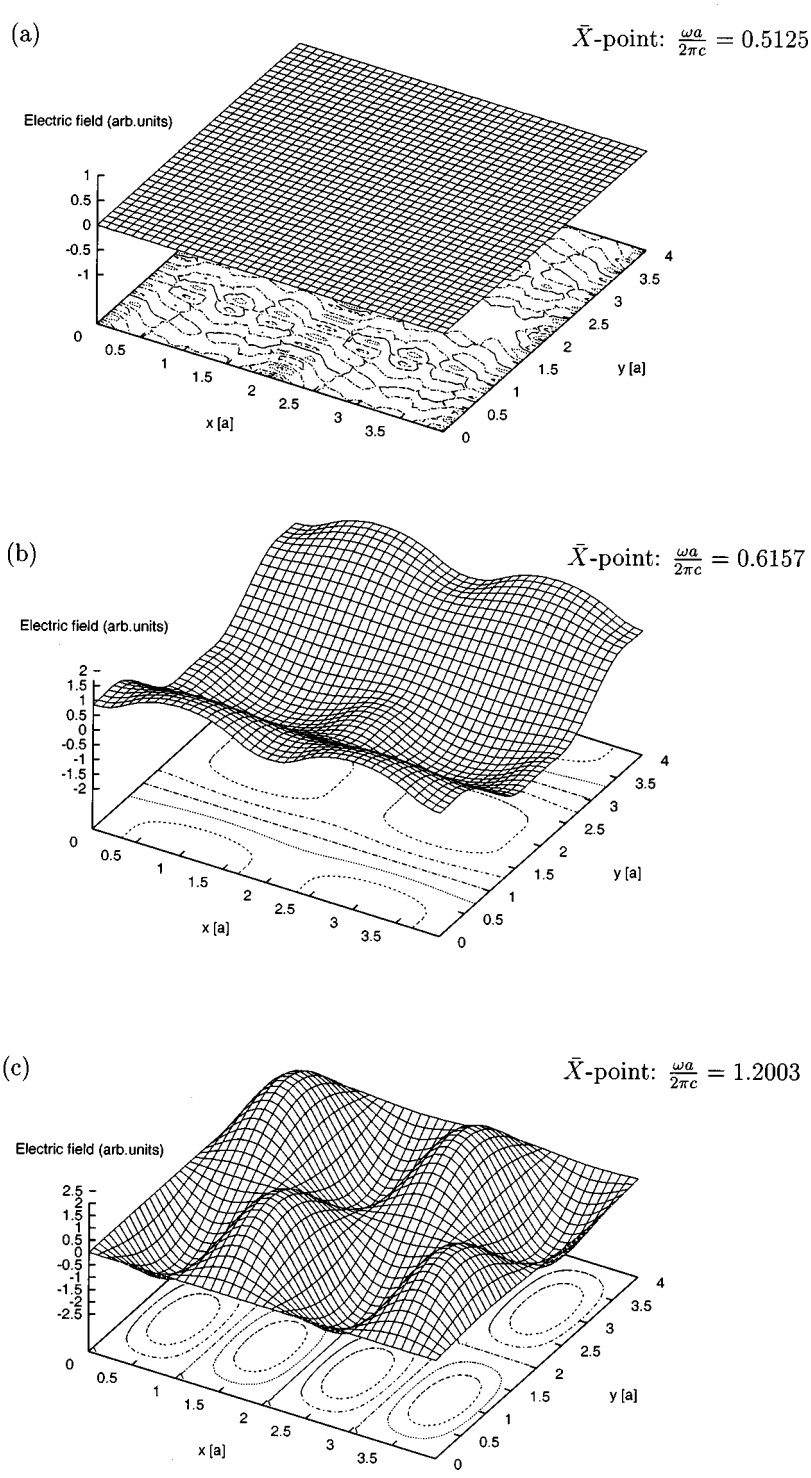

FIG. 5. The electric field distributions associated with the eigenfunctions and eigenvalues that correspond to the photonic band structure shown in Fig. 1, evaluated at the $\bar{X}$ point in the first Brillouin zone that correspond to the three lowest bands with the frequencies (a) $\omega a/2\pi c = 0.5125$, (b) $\omega a/2\pi c = 0.6157$, and (c) $\omega a/2\pi c = 1.2003$.

The spatial distribution of the intensity of the electric field that corresponds to the lowest frequency band at $\mathbf{k}_{\|} = (0.5,0.5)\pi/a$, shown in Fig. 8(a), displays fully symmetric behavior, which belongs to the irreducible representation A of the point group C_2. In Figs. 8(b) and 8(c) we present the intensities of the electric field associated with the second and third lowest frequencies at $\mathbf{k}_{\|} = (0.5,0.5)\pi/a$, that display field patterns that belong to the irreducible representations B and A of the point group C_2. From these results we find that all three lowest frequency bands are not significantly affected by the presence of dissipation.

In Fig. 9(a), we present the distributions of the intensity of the electric field associated with the lowest frequency band at the $\bar{\Gamma}$ point. We again observe that the nature of the spatial distribution of the intensity of the electric field associated with this nondegenerate mode is not significantly different

TABLE I. The irreducible representations in the first Brillouin zone for electromagnetic waves propagating in a two-dimensional photonic-crystal based on a square lattice.

Wave vector $\mathbf{k}_\parallel$	Symmetry	$\omega a/2\pi c$	Representation
Γ	C_{4v}	0	A_1
		1	A_1+B_1+E
		$\sqrt{2}$	A_1+B_2+E
		2	A_1+B_1+E
$\bar{M}$	C_{4v}	$1/\sqrt{2}$	A_1+B_2+E
		$\sqrt{10}/2$	$A_1+A_2+B_1+B_2+2E$
$\bar{X}$	C_{2v}	1/2	A_1+B_1
		$\sqrt{5}/2$	$A_1+A_2+B_1+B_2$
		3/2	A_1+B_1
		$\sqrt{13}/2$	$A_1+A_2+B_1+B_2$

from that found in the nondissipative case, while the presence of dissipation remarkably affects the nature of the spatial distribution of the intensity of the electric field associated with the third lowest doubly degenerate state of E symmetry at the $\bar{\Gamma}$ point, which displays patterns that are symmetric with respect to the mirror planes $\sigma_v^{(1)}$ and $\sigma_v^{(2)}$, as shown in Figs. 9(b) and 9(c) and thus, reflect the symmetry of the basis functions $E^{(xz)}$ and $E^{(yz)}$ of the two-dimensional irreducible representation E of the point group C_{4v}.

In Fig. 10(a) we present the distribution of the intensity associated with the lowest frequency band at the $\bar{X}$ point with a field pattern of B_1 symmetry, which is symmetric with respect to the σ_v reflection and significantly differs from the vanishing field pattern that corresponds to this mode in the case of lossless rods. The intensities associated with the second and third lowest frequency bands shown in Figs. 10(b) and 10(c) resemble the lossless field patterns that belong to the A_1 and A_2 irreducible representations of the point group C_{2v}, respectively.

In order to acquire a deeper physical insight into the phenomena associated with the presence of dissipation represented by the remarkably different field patterns at the points of high symmetry in comparison to those found in the case of

TABLE II. The compability relations between the irreducible representations shown in Table I.

Representations at points of high symmetry	Representation along $\bar{M}$-$\bar{\Gamma}$	Representation along $\bar{\Gamma}$-$\bar{X}$
$\bar{\Gamma}(A_1)$	A	A
$\bar{\Gamma}(A_2)$	B	B
$\bar{\Gamma}(B_1)$	B	A
$\bar{\Gamma}(B_2)$	A	B
$\bar{\Gamma}(E)$	$A+B$	$A+B$
$\bar{M}(A_1),\bar{M}(B_2)$	A	
$\bar{M}(A_2),\bar{M}(B_1)$	B	
$\bar{M}(E)$	$A+B$	
$\bar{X}(A_1),\bar{X}(B_1)$		A
$\bar{X}(A_2),\bar{X}(B_2)$		B

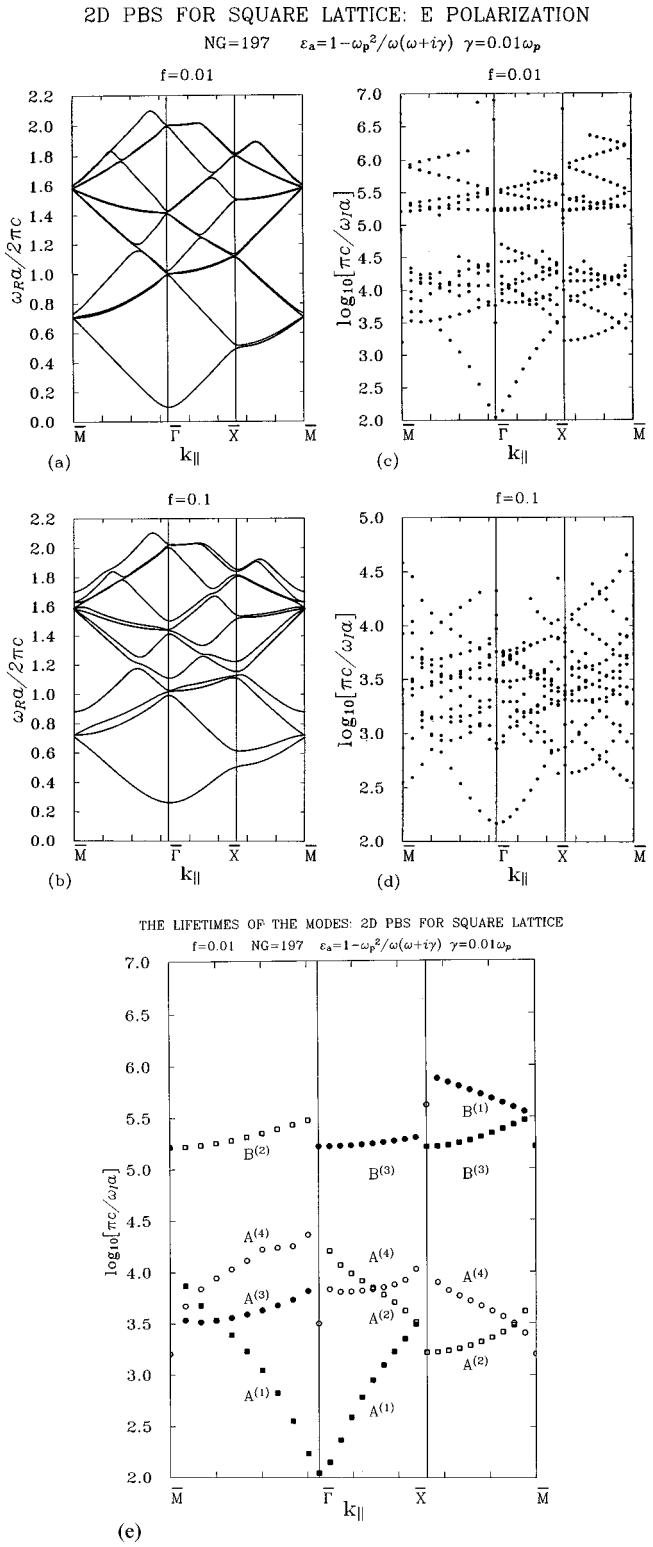

FIG. 6. The photonic band structure of a square lattice of lossy metal cylinders in vacuum obtained by the linearization technique. E polarization, (a) $f=0.01$, (b) $f=0.1$, and the lifetime of the modes associated with the photonic band structures shown in (a) and (b); (c) $f=0.01$, (d) $f=0.1$. The number of plane waves used in these calculations is $NG=197$; (e) the formation of the separated branches of the lifetimes associated with four lowest frequency bands, when $f=0.01$. The bands are indicated in increasing order by full squares, open squares, full circles and open circles, respectively.

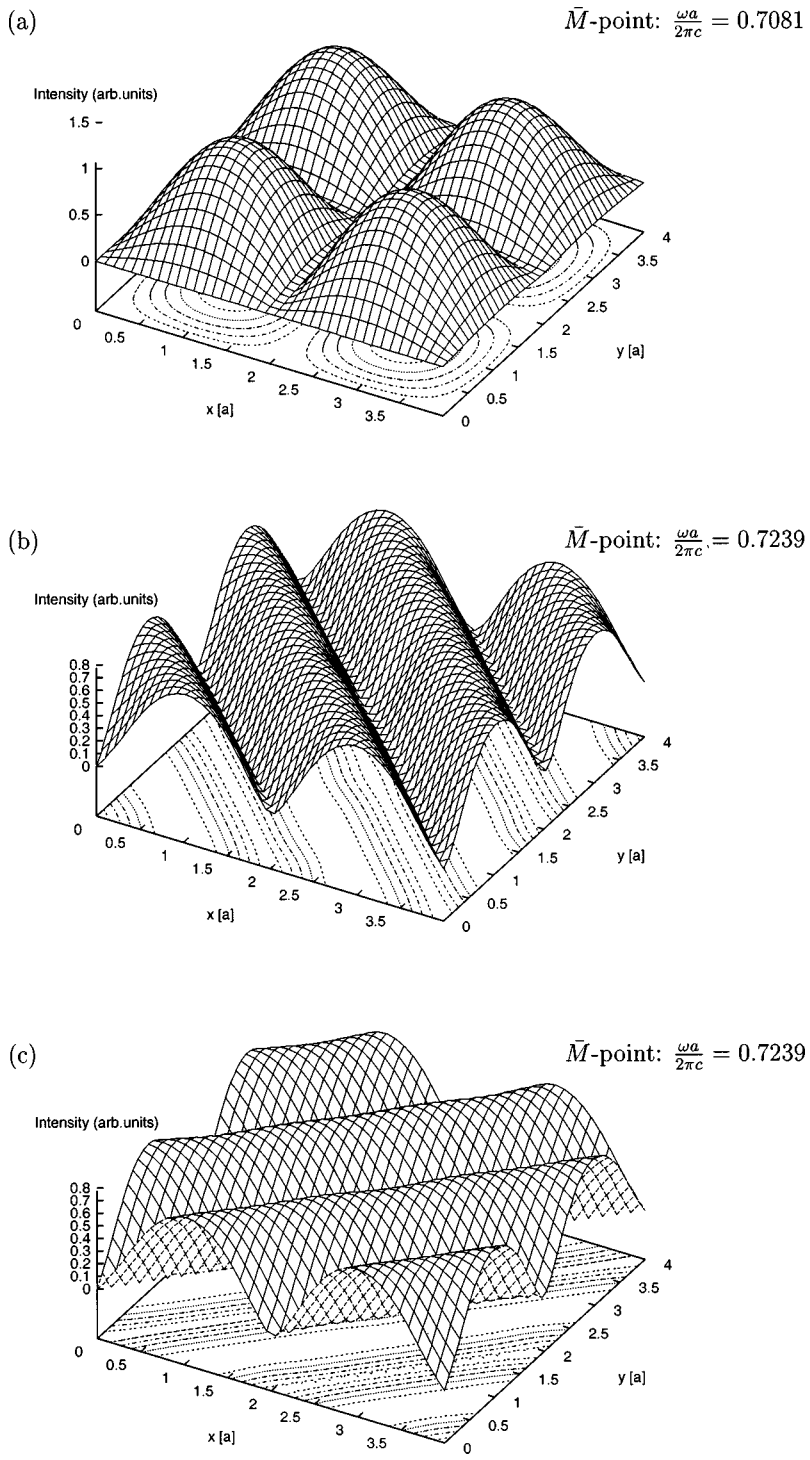

FIG. 7. The intensity of the electric field distributions associated with eigenvectors that correspond to complex eigenvalues of the photonic band structure shown in Figs. 6(b) and 6(d), evaluated at the $\bar{M}$ point of the first Brillouin zone, which correspond to the lowest band with the frequency (a) $\omega a/2\pi c = 0.7081$, and to the orthogonal eigenvectors associated with the second lowest doubly degenerate mode with the frequency (b) and (c) $\omega a/2\pi c = 0.7239$.

lossless rods, we plot both the real and imaginary components of the electric fields associated with the modes that are significantly affected by the presence of damping. First, we display a typical field pattern associated with a mode that is negligibly affected by the presence of damping. In this case, the real component of the electric field is much larger than the imaginary component as is demonstrated in Figs. 11(a) and 12(a), in which we show the field patterns that correspond to the real and imaginary components of the electric field associated with the lowest frequency band at the $\bar{M}$ point.

Next, we display the field patterns that belong to the modes that exhibit the opposite behavior, viz., the magnitudes of the real components are negligible in comparison with the imaginary components of the electric field. In fact, this phenomenon is closely linked to the effect of the van-

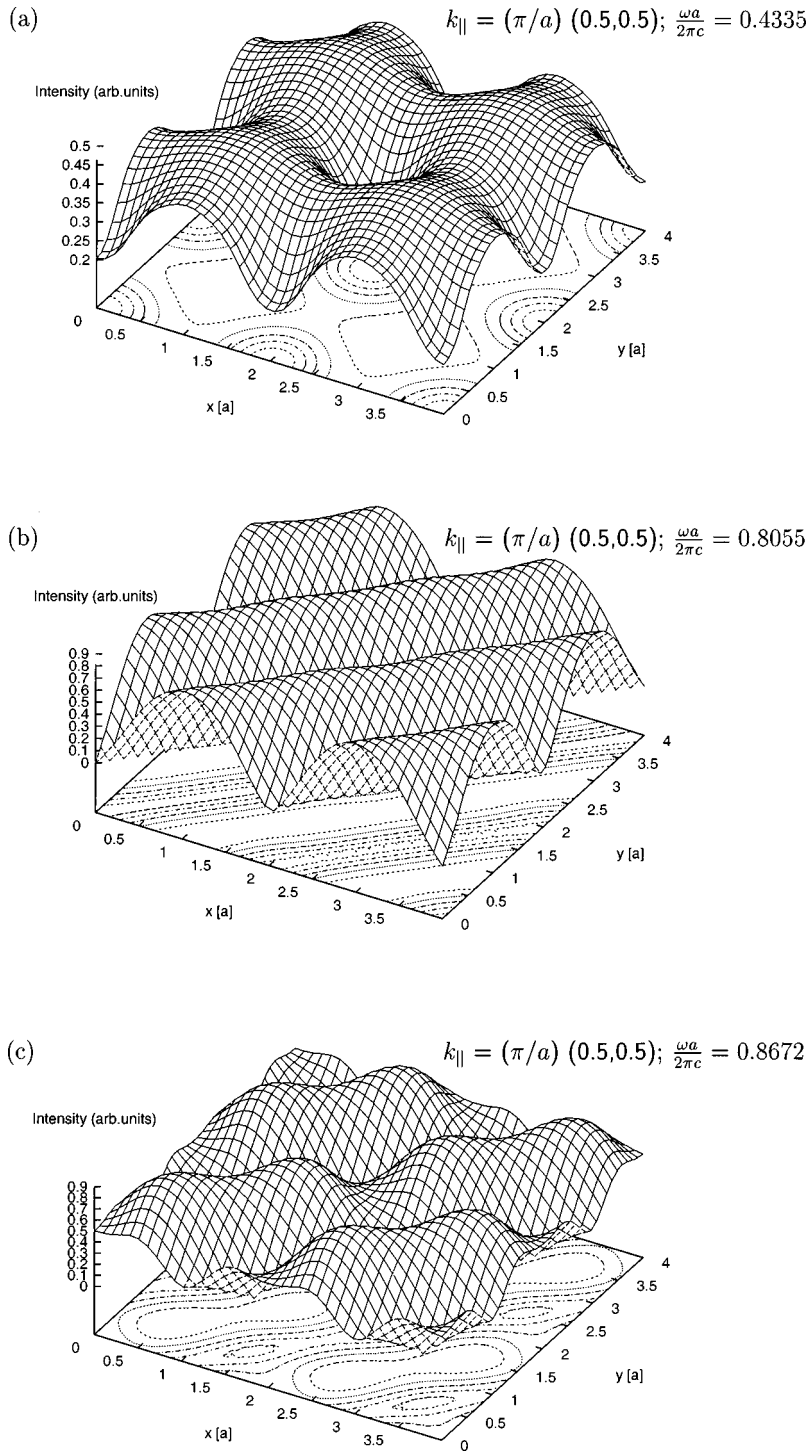

FIG. 8. The intensity of the electric field distributions associated with eigenvectors that correspond to complex eigenvalues of the photonic band structure shown in Figs. 6(b) and 6(d), evaluated at the $\mathbf{k}_{\|} = (0.5,0.5)\,\pi/a$ point of the first Brillouin zone, which correspond to the lowest band with the frequency (a) $\omega a/2\pi c = 0.4335$, to the second lowest band with the frequency (b) $\omega a/2\pi c = 0.8055$, and to the third lowest mode with the frequency (c) $\omega a/2\pi c = 0.8672$.

ishing amplitude of the electric fields found for the doubly degenerate modes of E symmetry at the M and Γ points, and for the nondegenerate band associated with the lowest frequency band at the X point. To illustrate this behavior, we display the field patterns associated with the real—Figs. 11(b) and 11(c)—and imaginary—12(b) and 12(c)—components of the electric field patterns, which correspond to the doubly degenerate modes of E symmetry at the M point, and the field patterns associated with the real—Figs. 13(a) and 13(b)—and imaginary—14(a) and 14(b)—components of the electric field that correspond to the doubly degenerate modes of E symmetry at the Γ point. In Figs.

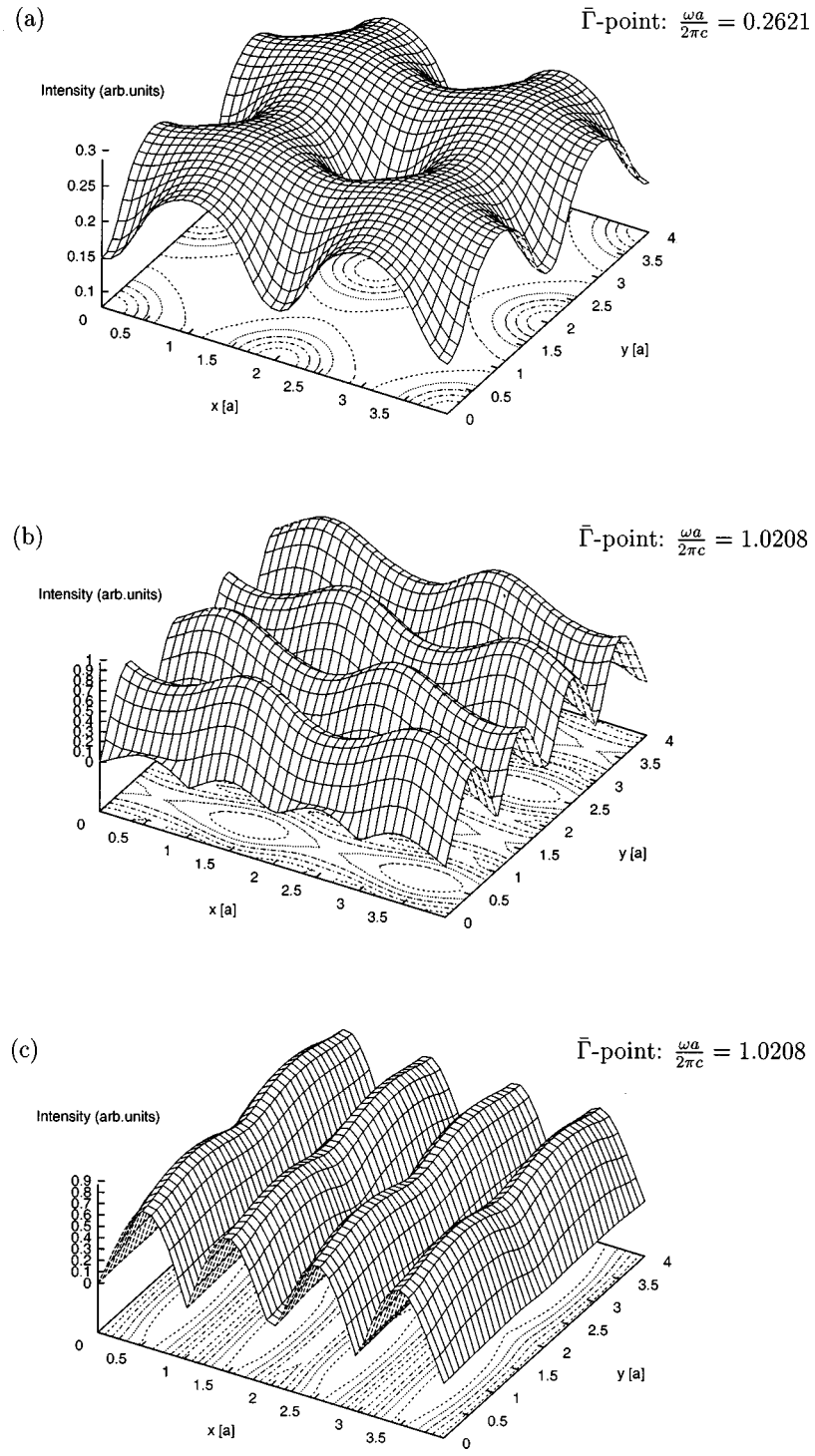

FIG. 9. The intensity of the electric field distributions associated with eigenvectors that correspond to the complex eigenvalues of the photonic band structure shown in Figs. 6(b) and 6(d), evaluated at the $\bar{\Gamma}$ point in the first Brillouin zone that correspond to the lowest band with the frequency (a) $\omega a/2\pi c = 0.2612$, and to the orthogonal eigenvectors associated with the third lowest band with the frequency (b) and (c) $\omega a/2\pi c = 1.0208$.

13(c) and 14(c) we display the real and imaginary parts of the field associated with the nondegenerate lowest frequency band at the $\bar{X}$ point, respectively.

C. Group velocity associated with the eigenmodes propagating in a system of metallic rods without dissipation

By inspecting the group velocity pattern as a function of the wave vector $\mathbf{k}_{\|}$ in the first Brillouin zone we directly obtain information about the energy flux, induced electric field, and the Poynting vector. While the amount of the energy flow is directly proportional to the group velocity v_g, the magnitude of the Poynting vector and the intensity of the induced electric field are proportional to $1/v_g$ and $1/v_g^2$, respectively.[14] To analyze these quantities we evaluate the group velocity associated with the eigenmodes that propagate through the system consisting of lossless metallic cylin-

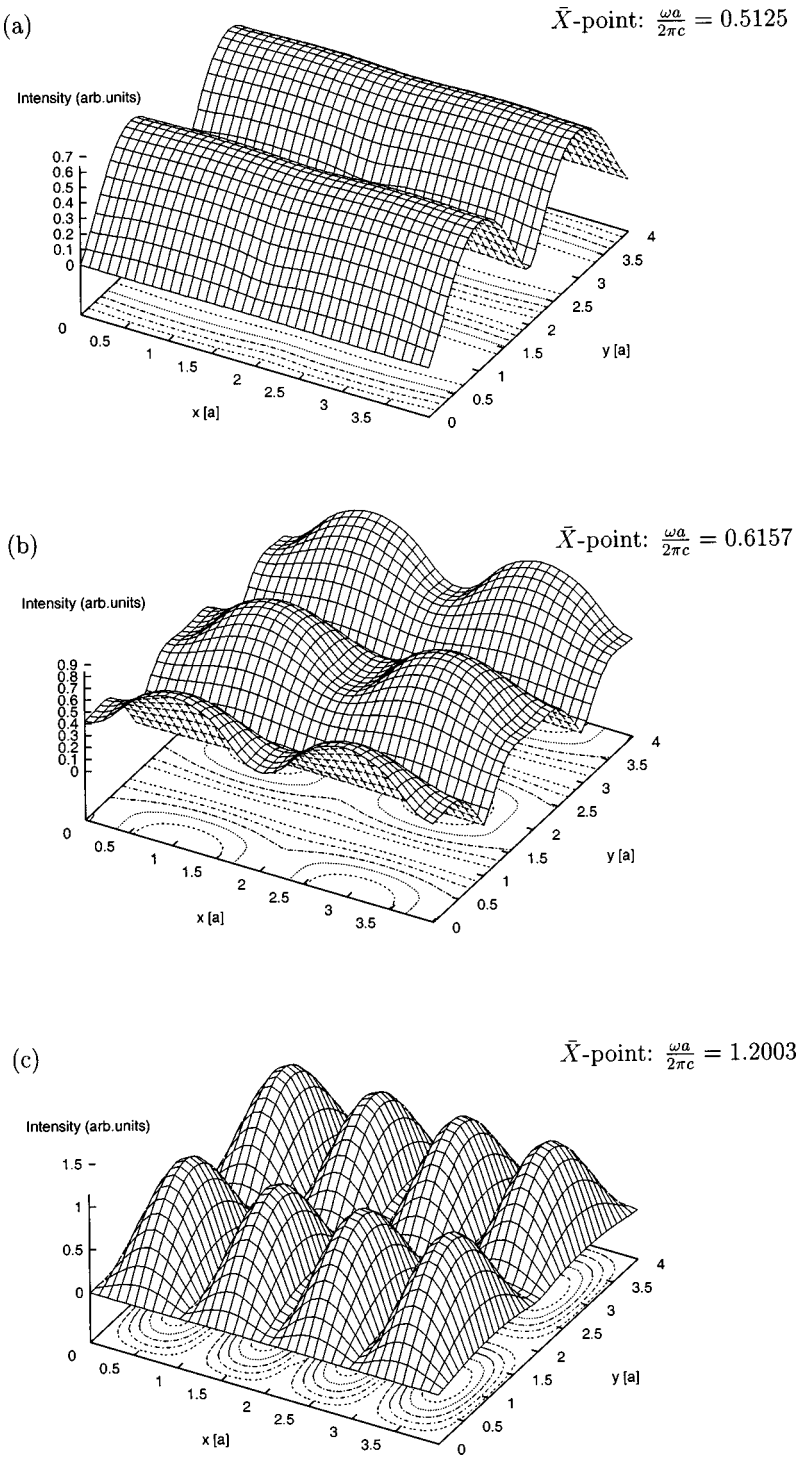

FIG. 10. The intensity of the electric field distributions associated with eigenvectors that correspond to complex eigenvalues of the photonic band structure shown in Figs. 6(b) and 6(d), evaluated at the $\bar{X}$ point of the first Brillouin zone, which correspond to the lowest band with the frequency (a) $\omega a/2\pi c = 0.5125$, to the second lowest band with the frequency (b) $\omega a/2\pi c = 0.6157$, and to the third lowest mode with the frequency (c) $\omega a/2\pi c = 1.2003$.

ders considered in Sec. II. To calculate the dependence of the group velocity on the wave vector we employ Eq. (2.19) into which the matrix $M_E(\mathbf{k}_\parallel + \mathbf{G}_\parallel | \mathbf{k}_\parallel + \mathbf{G}'_\parallel)$ given by Eq. (2.18), that describes the dispersion law for E polarized electromagnetic waves in the nondissipative system, is substituted. The results are presented as patterns associated with the individual bands, which show the dependence of the group velocity on the two-dimensional wave vector $\mathbf{k}_\parallel$, which is sampled every $\pi/15a$ in the first Brillouin zone, where a is the lattice constant.

In Figs. 15(a)–15(c), we present the distribution of the absolute value of the group velocity associated with the three lowest bands, which correspond to the dispersion curves shown in Fig. 1. The most notable feature of the group ve-

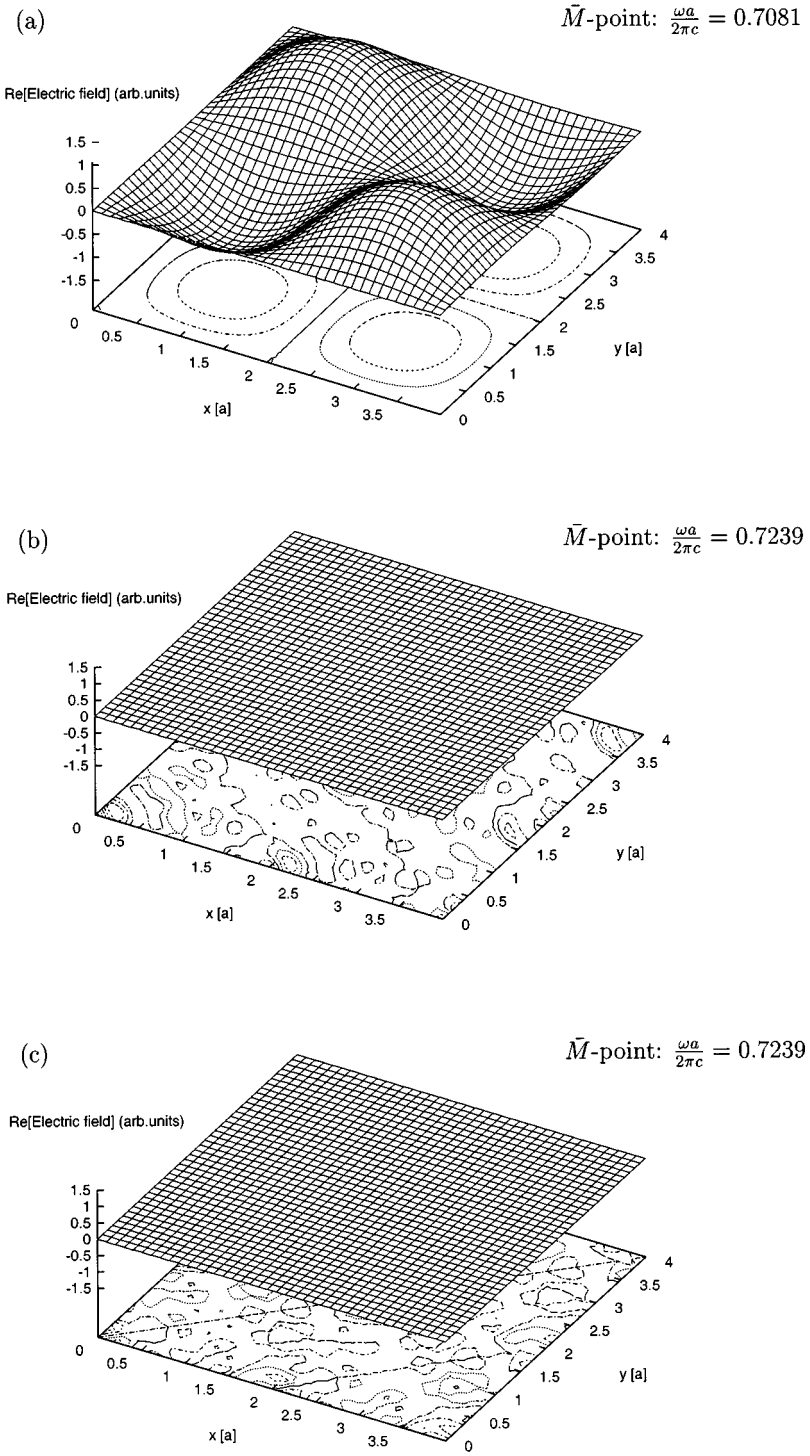

FIG. 11. The real part of the electric field distributions associated with eigenfunctions that correspond to the complex eigenvalues of the photonic band structure shown in Figs. 6(b) and 6(d), evaluated at the $\bar{M}$ point in the first Brillouin zone, which correspond to the lowest band with the frequency (a) $\omega a/2\pi c = 0.7081$, and to the second lowest doubly degenerate mode with the frequency (b), (c) $\omega a/2\pi c = 0.7239$.

locity associated with the lowest band depicted in Fig. 15(a) is its nonmonotonic dependence on the wave vector, with a vanishing amplitude at the $\bar{\Gamma}$ point and near the boundaries of the first Brillouin zone. The distribution of the group velocity of each of the modes reflects the symmetry and the characteristic features associated with each of the bands, and determines the directions along which the group velocity is reduced or tends to zero. Specifically, the group velocity that corresponds to the second and third lowest bands reveals a reduced amplitude along the $\bar{\Gamma}$-$\bar{M}$ and $\bar{\Gamma}$-$\bar{X}$ directions in the first Brillouin zone, respectively.

We have shown in a previous paper[7] that the width of the gap, which occurs between the first and second lowest bands is a nonmonotonic function of the filling fraction. The effect of increasing the filling fraction on the distribution of the group velocity is demonstrated in Figs. 16(a)–16(c), in

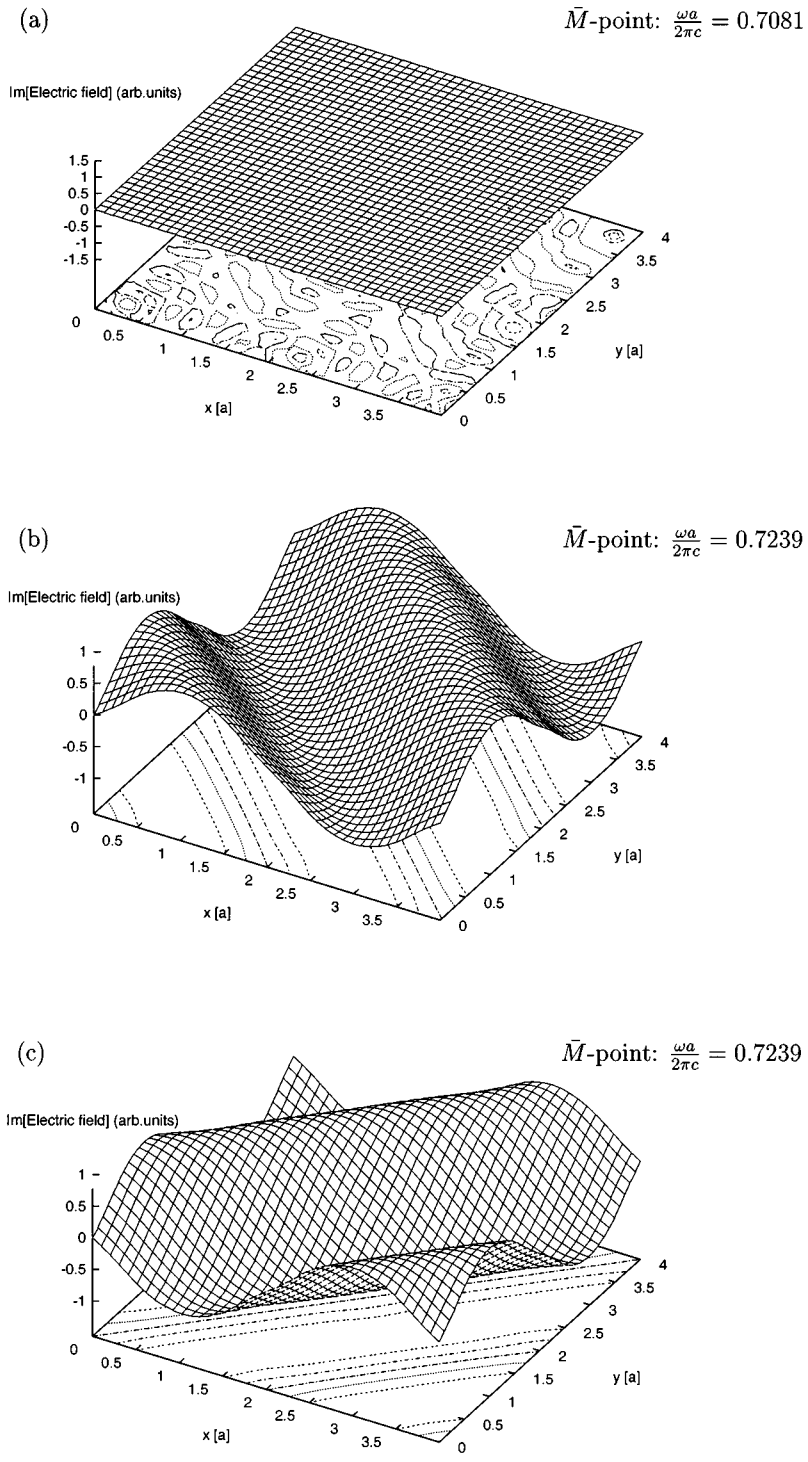

FIG. 12. The imaginary part of the electric field distributions associated with eigenfunctions that correspond to the complex eigenvalues of the photonic band structure shown in Figs. 6(b) and 6(d), evaluated at the $\bar{M}$ point in the first Brillouin zone, which correspond to the lowest band with the frequency (a) $\omega a/2\pi c = 0.7081$, and to the second lowest doubly degenerate mode with the frequency (b), (c) $\omega a/2\pi c = 0.7239$.

which we present the group velocity associated with the three lowest bands when the filling fraction of the rods corresponds to the maximum value of the band gap, viz., $f = 0.7$. The patterns shown in the latter figure resemble the group velocities that correspond to the case when the filling fraction $f = 0.1$, except that their magnitudes are reduced due to the flattened nature of the dispersion curves.

IV. DISCUSSION AND CONCLUSIONS

In this paper, we have analyzed the spatial distribution of the electric fields and group velocities associated with the eigenmodes that correspond to the photonic band structure of electromagnetic waves propagating through periodic two-dimensional systems containing both lossless and lossy me-

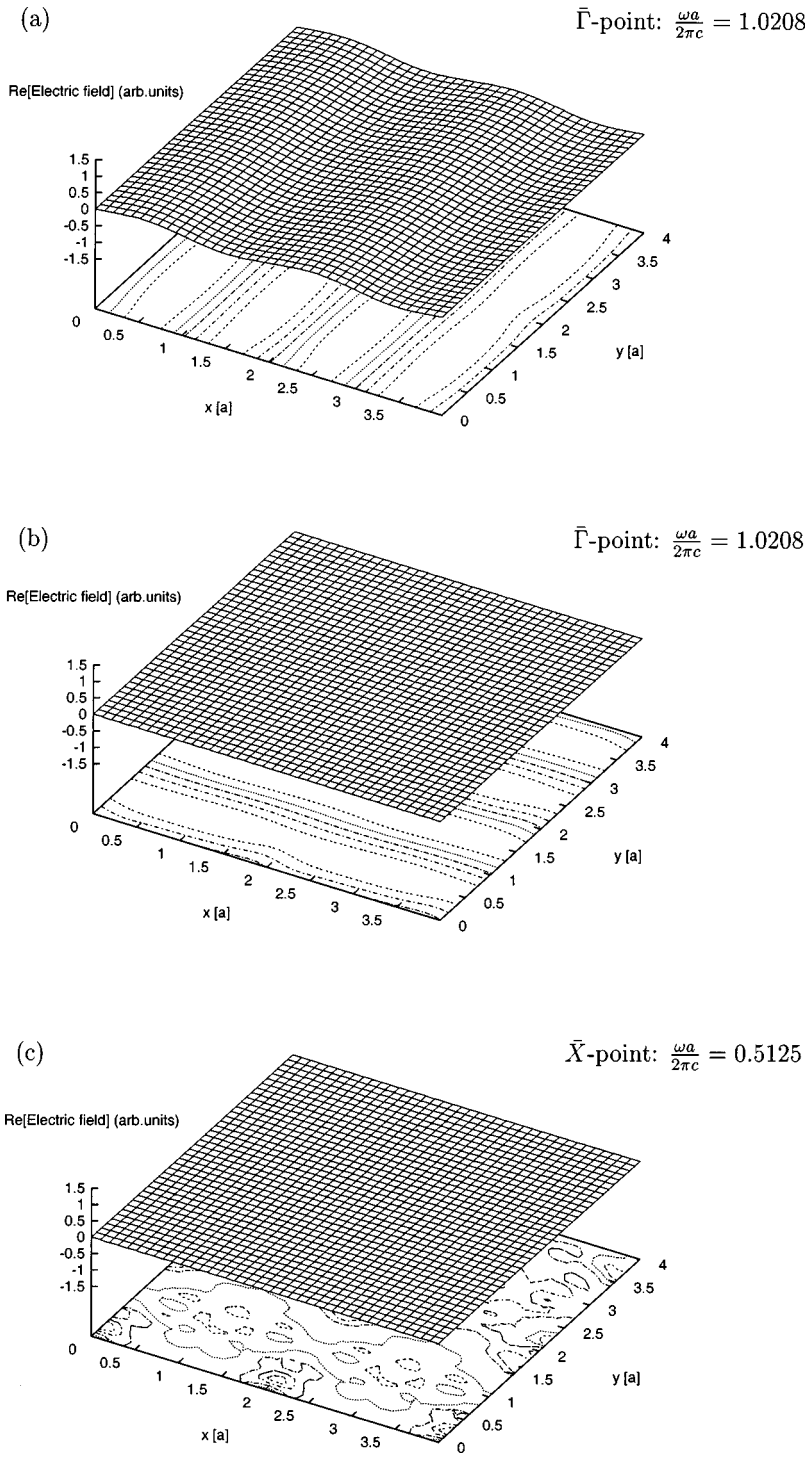

FIG. 13. The real part of the electric field distributions associated with eigenfunctions that correspond to the complex eigenvalues of the photonic band structure shown in Figs. 6(b) and 6(d), evaluated at the $\bar{\Gamma}$ point in the first Brillouin zone, which correspond to the third lowest doubly degenerate band with the frequency (a), (b) $\omega a/2\pi c = 1.0208$, and to the lowest nondegenerate mode at the $\bar{X}$ point with the frequency (c) $\omega a/2\pi c = 0.5125$.

tallic components characterized by frequency dependent dielectric functions given by Eqs. (2.1) and (2.2), respectively. Our study is based on the calculation of the (complex) photonic band structure by the plane-wave approach developed by the present authors[7,5,15] and the application of this method to the calculation of the group velocity presented in Sec. II. We first studied the nature and symmetry properties of the eigenvectors at the points of high symmetry in the first Brillouin zone. We considered both lossless and lossy metallic cylinders to investigate how the eigenfunctions are affected by the presence of damping, and to obtain a deeper physical insight into the interesting features observed in the complex photonic band structure, in particular in the lifetimes of the modes determined from its imaginary part. Then, we evaluated the group velocities associated with the individual bands as functions of the two-dimensional wave vector $\mathbf{k}_{\|}$ to exam-

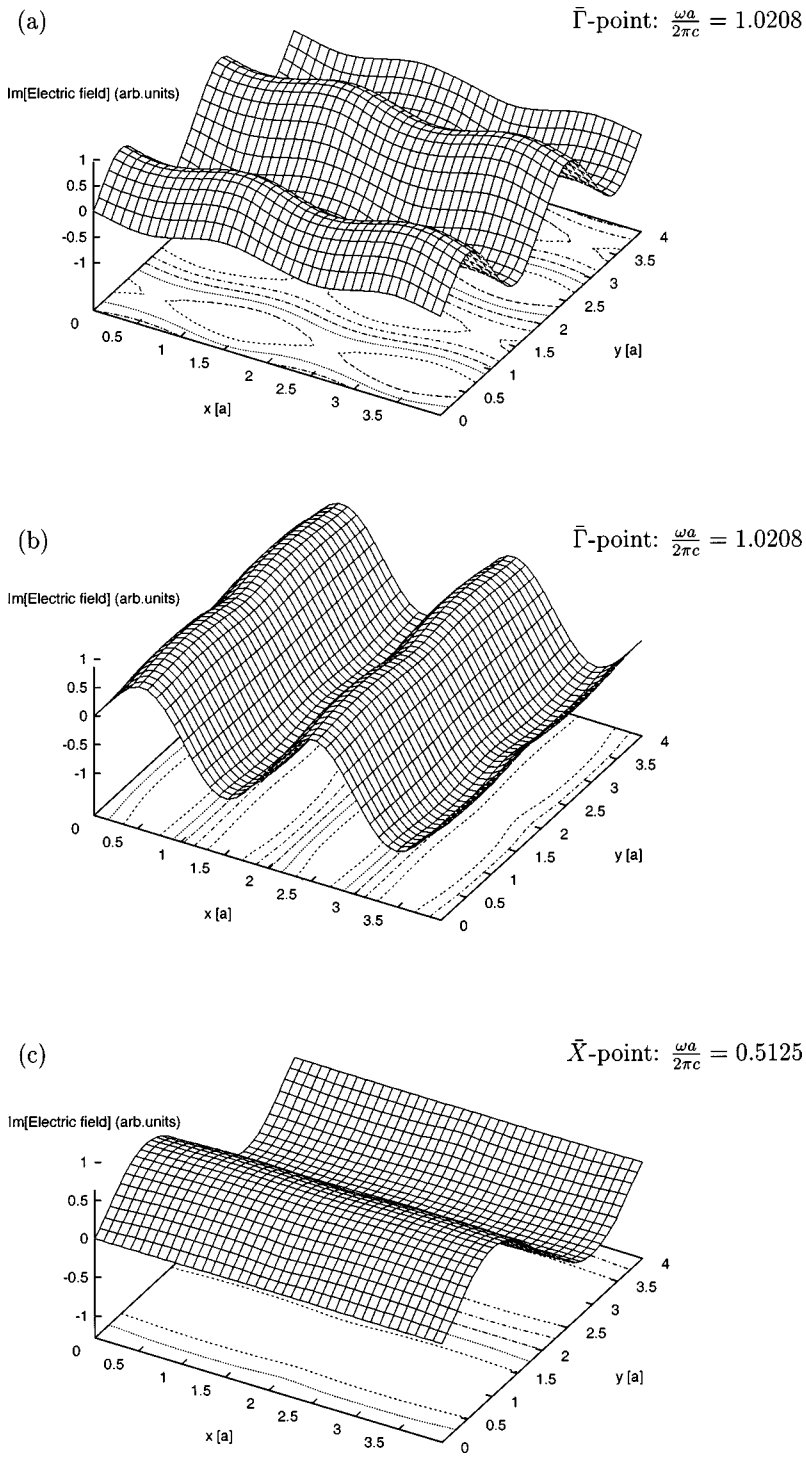

FIG. 14. The real part of the electric field distributions associated with eigenfunctions that correspond to the complex eigenvalues of the photonic band structure shown in Figs. 6(b) and 6(d), evaluated at the $\bar{\Gamma}$ point in the first Brillouin zone, which correspond to the third lowest doubly degenerate band with the frequency (a), (b) $\omega a/2\pi c = 1.0208$, and to the lowest nondegenerate mode at the $\bar{X}$ point with the frequency (c) $\omega a/2\pi c = 0.5125$.

ine the energy flow in the system with lossless components.

By evaluating the spatial distribution of the electric field associated with the eigenmodes propagating through the nondissipative system we have identified the symmetry of the bands at the points of high symmetry and along the high symmetry directions in the first Brillouin zone, even in cases when a definite symmetry cannot be assigned by group theory. We have examined the individual bands, in particular with respect to the interpretation of the features observed in the photonic band structures in the systems characterized by a frequency-dependent dielectric function. The patterns associated with the individual eigenvectors at the high-symmetry points of the first Brillouin zone possess the symmetry properties predicted by group theory. As a notable feature, our results predict that the amplitude of the electric field associated with some of the eigenmodes vanishes. Specifically, we

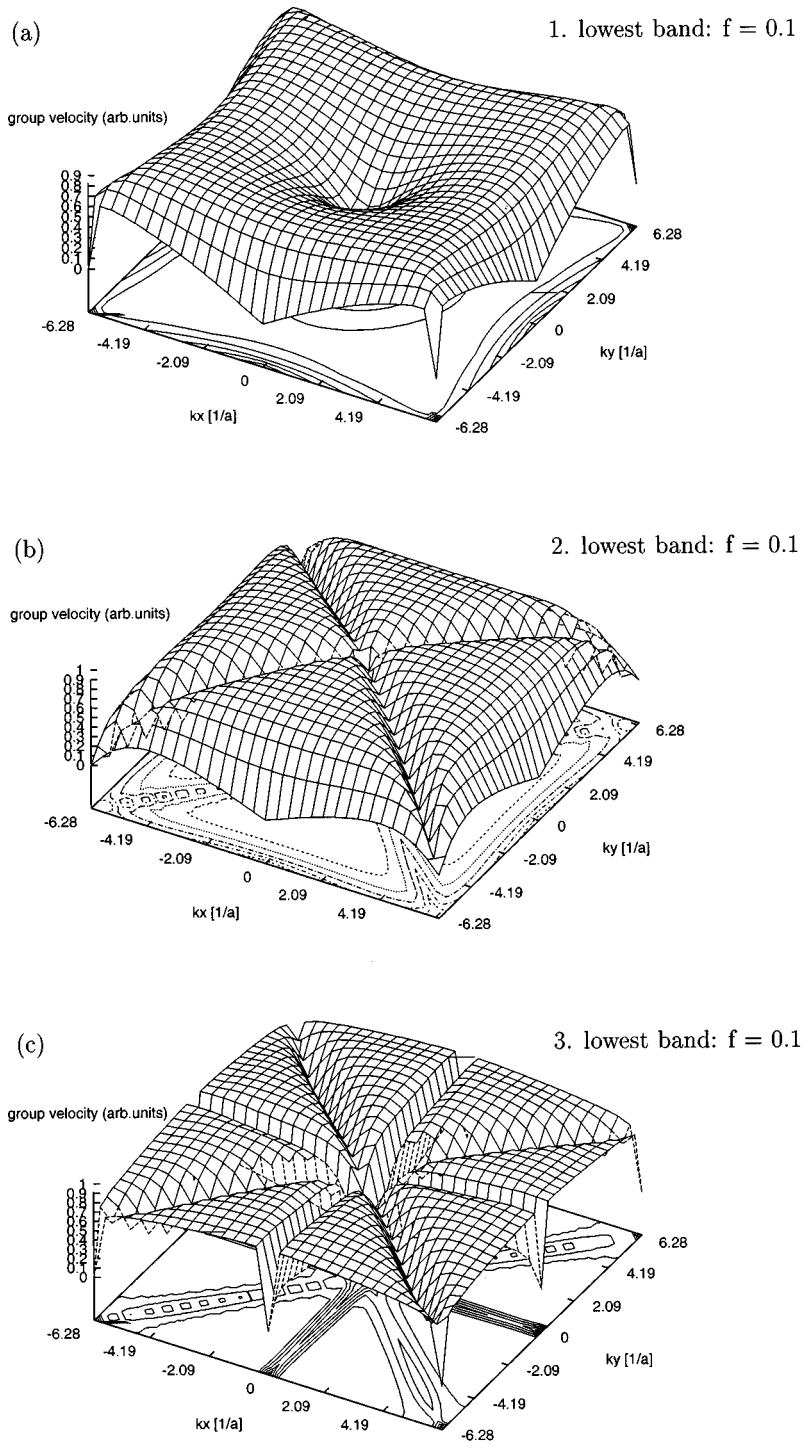

FIG. 15. The group velocity of the three lowest bands that correspond to the photonic band structure shown in Fig. 1, when the filling fraction of the rods is $f=0.1$ evaluated in the first Brillouin zone as a function of the two-dimensional wave vector $\mathbf{k}_{\|}$. The distribution of the group velocities associated with the individual bands is tabulated every $\pi/15a$ in the first Brillouin zone, where a is the lattice constant.

found a vanishing amplitude of the electric fields associated with the orthogonal eigenvectors which correspond to doubly degenerate modes of E symmetry at the M and Γ points. A vanishingly small amplitude of the electric field was also found in the case of the lowest frequency band at the X point. In order to explore the origin of this behavior we have inspected the eigenfunctions, and have found that the vanishing of the electric field associated with the doubly degenerate states of E symmetry at the Γ point is due to the opposite signs of the coefficients of the plane waves in the expansion (2.11) within each of the shells of reciprocal lattice vectors, while the vanishing of the electric fields associated with the doubly degenerate modes of E symmetry at the M point and the nondegenerate mode of B_1 symmetry at the Γ point is

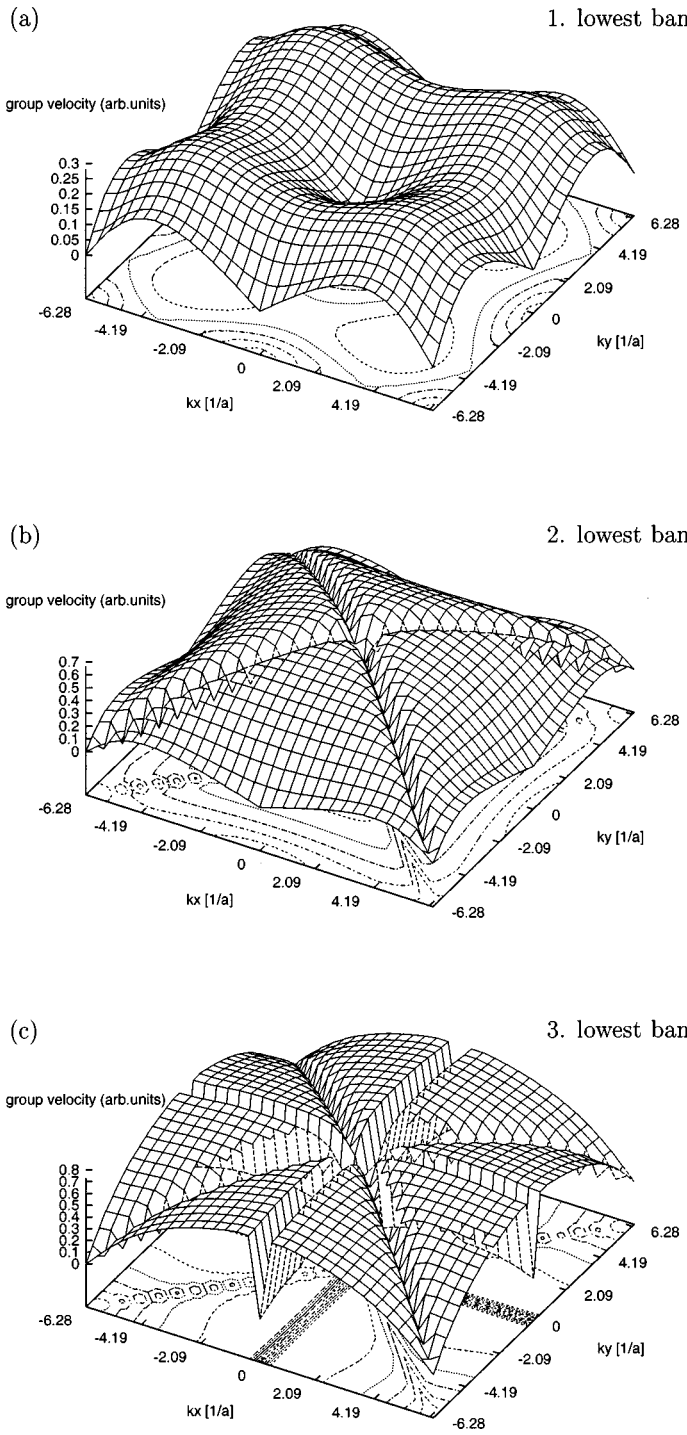

FIG. 16. The same as in Fig. 15, except that the filling fraction is $f=0.7$.

due to the alternating signs of the terms from the shells of increasing order, which converge to zero as the distance from the origin to a shell goes to infinity.

We have analyzed the behavior of the coefficients produced by the diagonalization procedure associated with the doubly degenerate states in the vicinity of the $\overline{\Gamma}$ point and compared them to those obtained by using a projection operator technique. We found that the symmetrized plane waves produced by the latter method are consistent with those generated by the numerical procedure. Thus, we think that the vanishing of the electric field at the $\overline{\Gamma}$ point is not an artifact of the diagonalization procedure, and represents a real effect. To interpret this effect we suggest solutions of Eqs. (2.11) and (2.23) that yield a vanishing field with a nonzero frequency represent trivial solutions, indicating that a mode with such a frequency is absent in the system.

The analysis of the eigenfunctions associated with the modes propagating through a nondissipative system has been used as the starting point for exploring the relation between the dispersion curves and the components of the complex

valued photonic band structure, which describes the propagation of electromagnetic waves in systems with metallic components characterized by a complex frequency-dependent dielectric function. We have found that the dispersion curves determined from the resulting complex photonic band structure obtained by the linearization technique are negligibly changed when a damping term with a typical value for metals $\gamma=0.01\omega_p$ is used. The presence of dissipation, however, significantly affects the nature of the eigenfunctions. In contrast to the nondissipative system, the diagonalization of the non-Hermitian matrix yields right and left eigenvectors. We have proved that both right and left eigenvectors are equivalent and therefore we can restrict ourselves to either of the two eigenvectors.

The analysis of our results reveals that the intensities of the electric fields associated with the modes resemble the field patterns associated with the corresponding modes in the nondissipative case. The presence of dissipation, however, significantly affects the nature of the spatial distribution of the electric field at the points of high symmetry at which the electric field in the case of lossless rods vanishes. Specifically, we have shown that the complex electric fields associated with the doubly degenerate states of E symmetry at the M and Γ points and with the nondegenerate states of B_1 symmetry at the X point possess a dominant imaginary part. In contrast to the field patterns associated with the doubly degenerate modes in the nondissipative system that vanish, the intensity of the electric field associated with the degenerate modes at the M and Γ points, determined by diagonalization of the non-Hermitian matrix $\overleftrightarrow{W}(\vec{G}_\parallel|\vec{G}'_\parallel)$, display patterns that reflect the symmetry of the basis functions $E^{(xz)}$, $E^{(yz)}$ of the two-dimensional irreducible representation E of the point group C_{4v}.

By studying the spatial distribution of the electric field associated with the eigenmodes propagating through the two-dimensional system consisting of lossy metallic rods we obtained a deeper physical insight into the effects exhibited by the lifetimes of the modes. We have shown that the existence of the separated branches of the lifetimes is due to the symmetry of the modes. The lifetimes associated with the modes of A symmetry belong to the lower band, while those that correspond to the antisymmetric uncoupled modes give rise to the upper band. The existence of branches of the lifetimes is closely linked to the difference in the spatial variation of the fields associated with the symmetric modes, which exhibit predominant variation in the region of the rods, while the variation of the uncoupled modes occurs mostly between the rods. Consequently, for the lifetimes determined from the imaginary part of the complex photonic band structure and, therefore, for small values of the filling fraction of the rods, the difference between the spatial variation of the symmetric and antisymmetric modes tends to affect the difference between the imaginary components of the complex eigenvalues more significantly than in the case of the real components, and implies the existence of separated branches of the lifetimes. Such behavior is consistent with a simple physical explanation, which assumes longer lifetimes of the modes that are mostly extended in the region with low dielectric constant than of those that are more localized in the region of the rods. Specifically, the modes with the dominant spatial variation in the air region have a negligible overlap with the thin metal rods, which act as a repulsive potential, and exhibit smaller dissipation than those whose variation is localized at the positions of the rods and have a significantly larger overlap with the rods and therefore dissipate their energy into the system to a greater degree. It is worth emphasizing that this effect is predicted to occur when the filling fraction of the metallic rods is smaller than 5%.

The eigenvalues and eigenvectors determined in the photonic band-structure calculations have been utilized to calculate the group velocities of the individual bands, which allow examining the flow of energy associated with each of the eigenmodes. We have shown that the dependence of the group velocities on the wave vector $\mathbf{k}_\parallel$ reveals a vanishing amplitude at the symmetry points and along the high-symmetry directions in the first Brillouin zone. This effect may have important practical applications. It has been demonstrated that in a one-dimensional photonic band-gap structure a vanishing group velocity increases the optical path due to the multiple reflections of photons near the photonic band gap, and can lead to the enhancement of gain in an active medium.[16] The vanishing group velocity at a photonic band edge may also lead to the enhancement of nonlinear processes compared with their strengths in a uniform material, as was shown in the case of the enhancement of the induced second-harmonic field intensity caused by a vanishing group velocity near the photonic band edge in a two-dimensional photonic crystal in the presence of nonlinearity.[17] The distribution of the group velocities associated with the bands displays a rich variety of patterns as the band number increases, and the nodal structure of the higher frequency bands becomes more complicated. This strong directional dependence indicates the existence of channels of energy flow, which may prove be an effective mechanism in controlling photon propagation through a photonic crystal.

The propagation of electromagnetic waves in absorbing media is described by a complex valued dispersion law, and the associated group velocities also become complex. Let us first consider the components of the electric field and the complex group velocity associated with the right eigenvector. While the real part of the complex group velocity $\nabla_{\mathbf{k}_\parallel}\mathrm{Re}[\omega_\mu(\mathbf{k}_\parallel)]$ determines the propagation direction of the maximum energy density, the imaginary part is related to the directions in which the maximum dissipation of the energy density occurs. It can be explicitly expressed as $\nabla_{\mathbf{k}_\parallel}\mathrm{Im}[\omega_\mu(\mathbf{k}_\parallel)]=[1/2\tau_\mu(\mathbf{k}_\parallel)^2]\nabla_{\mathbf{k}_\parallel}\tau_\mu(\mathbf{k}_\parallel)$, and represents the rate of dissipation of the photon's energy into the system in the direction of the maximum dissipated energy density, where $\tau_\mu(\mathbf{k}_\parallel)$ is the lifetime associated with the μth band defined in Eq. (2.15).[18]

This topic is part of a more general problem concerned with the properties of the macroscopic fields inside dielectrics, which has been studied both theoretically and experimentally. One of the crucial questions raised is that of the general expression for the Poynting vector in scattering or absorbing media. It has been shown that if a Gaussian wave packet is chosen for the initial wave packet $\Psi_0(r)$, then the propagation direction of the maximum of the energy density is determined by the real part of the group velocity, and

inhomogeneous, strongly scattering media can be regarded as absorbing media, when the ensemble-averaged amplitude is considered.[19,20] To our knowledge, the relation between the Poynting vector and the group velocities, which constitute the crucial quantities describing the propagation of electromagnetic waves in absorbing photonic crystals, has not been addressed as yet, and will be investigated in a forthcoming publication.

ACKNOWLEDGMENTS

The work of V.K. was supported by the Japanese Society for Promotion of Science, and in part by the Czech Academy of Sciences Grant No. 202/96/1239. V.K. wishes to thank the Research Institute for Electronic Science, Hokkaido University, for its hospitality during a visit when this work was done. The work of A.A.M. was supported in part by NSF Grant No. DMR-9319404.

*Permanent address: Institute of Radio Engineering and Electronics, Czech Academy of Sciences, Chaberska 57, 182 51 Prague 8, Czech Republic.

[1] W. Robertson, G. Arjavalingam, R. D. Meade, K. D. Brommer, A. M. Rappe, and J. D. Joannopoulos, Phys. Rev. Lett. **68**, 2023 (1992).

[2] T. F. Krauss, R. M. De La Rue, and S. Brand, Nature (London) **383**, 699 (1996).

[3] K. Sakoda, Phys. Rev. B **52**, 7982 (1995).

[4] K. Sakoda, Phys. Rev. B **54**, 5732 (1996).

[5] V. Kuzmiak and A. A. Maradudin, Phys. Rev. B **55**, 7427 (1997).

[6] S. John, Phys. Rev. Lett. **58**, 2468 (1987).

[7] V. Kuzmiak, A. A. Maradudin, and F. Pincemin, Phys. Rev. B **50**, 16 835 (1994).

[8] M. Plihal and A. A. Maradudin, Phys. Rev. B **44**, 8565 (1991).

[9] P. Lancaster, *Lambda-Matrices and Vibrating Systems* (Pergamon, London, 1966), Chap. 4.

[10] L. D. Landau, E. M. Lifshitz, and L. P. Pitaevskii, *Electrodynamics of Continuous Media* (Pergamon, Oxford, 1984).

[11] M. Born and E. Wolf, *Principles of Optics* (Pergamon, Oxford, 1980).

[12] J. D. Jackson, *Classical Electrodynamics* (Wiley, New York, 1975).

[13] J. D. Joannopoulos, R. D. Meade, and J. N. Winn, *Photonic Crystals, Molding the Flow of Light* (Princeton University Press, Princeton, NJ, 1995).

[14] Y. R. Shen, *Principles of Nonlinear Optics* (Wiley, New York, 1984).

[15] V. Kuzmiak, A. A. Maradudin, and A. R. McGurn, Phys. Rev. B **55**, 4298 (1997).

[16] J. P. Dowling, M. Scalora, M. J. Bloemer, and C. M. Bowden, J. Appl. Phys. **75**, 1896 (1994).

[17] K. Sakoda and K. Ohtaka, Phys. Rev. B **54**, 5742 (1996).

[18] G. L. J. A. Rikken and B. A. van Tiggelen, Phys. Rev. Lett. **78**, 847 (1997).

[19] C. G. B. Garrett and D. E. McCumber, Phys. Rev. A **1**, 305 (1970).

[20] S. Chu and S. Wong, Phys. Rev. Lett. **48**, 738 (1982).